uOttawa

L'Université canadienne
Canada's university

FACULTÉ DES ÉTUDES SUPÉRIEURES ET POSTOCTORALES

uOttawa

L'Université canadienne
Canada's university

FACULTY OF GRADUATE AND POSDOCTORAL STUDIES

Daniel Gussin

AUTEUR DE LA THÈSE / AUTHOR OF THESIS

M.Sc. (Neuroscience)

GRADE / DEGREE

Department of Neuroscience

FACULTÉ, ÉCOLE, DÉPARTEMENT / FACULTY, SCHOOL, DEPARTMENT

Linear Coding of Dynamic Stimuli by Electroreceptor Afferents

TITRE DE LA THÈSE / TITLE OF THESIS

Len Maler

DIRECTEUR (DIRECTRICE) DE LA THÈSE / THESIS SUPERVISOR

CO-DIRECTEUR (CO-DIRECTRICE) DE LA THÈSE / THESIS CO-SUPERVISOR

EXAMINATEURS (EXAMINATRICES) DE LA THÈSE / THESIS EXAMINERS

Pierre Fortier

John Lewis

Gary W. Slater

Le Doyen de la Faculté des études supérieures et postdoctorales / Dean of the Faculty of Graduate and Postdoctoral Studies

Linear Coding of Dynamic Stimuli by Electroreceptor Afferents

Daniel Jeffrey Gussin

Department of Neuroscience

University of Ottawa, Ottawa, Ontario

July 29, 2008

This thesis is submitted as a partial fulfillment of the M.Sc. program in Neuroscience.

Your file Votre référence
ISBN: 978-0-494-46478-6
Our file Notre référence
ISBN: 978-0-494-46478-6

Statement of Contributions of Collaborators

The collaborators listed in the published manuscript "Gussin D, Benda J, Maler L. (2007) Limits of Linear Rate Coding of Dynamic Stimuli by Electroreceptor Afferents. *J. Neurophysiol.,* 97: 2917–2929." were Dr. Jan Benda and Dr. Leonard Maler. Dr. Jan Benda provided teaching on surgical procedures, recording techniques, and preparation of equipment as well as some baseline activity data. Dr. Leonard Maler provided the lab space and financial support as well as the mentorship, revisions and direction for this project. All the experimentation, mathematical analysis, and writing presented here were done by the author.

Abstract

To determine how sensory receptors respond to signal modulations, we estimated the frequency-intensity (f-I) curves of P-unit electroreceptors using 4 Hz random amplitude modulations (RAMs) and the covariance method (50 Hz RAMs). Both methods showed that P-units are linear encoders of stimulus amplitude with additive noise. The covariance method showed that a linear combination of eigenvectors representing the time-weighted stimulus intensity (E1) and its derivative (E2) could account for 92% of the total response variability. The low gain of the low frequency f-I curve implies that detection of prey would require integration over many receptors and time. Weak signals at the limit of behavioural thresholds could be detected if the animal were able to extract E1 from the population of responding P-units. We propose a tentative mechanism for this operation despite no evidence as to whether it is actually implemented in the nervous system of these fish.

Table of Contents

List of Figures

Legend

%	percent
%I	Relative intensity as a percent modulation of the maximum EOD amplitude
%ΔI	Relative change in intensity
A	covariance matrix
Ca^{2+}	calcium ion
cm	centimetre
C_{random}	covariance matrix at random times
C_{spike},	covariance matrix of all spike events
CV	coefficient of variation
E1	first eigenvector
E2	second eigenvector
ELL	electrosensory lateral line lobe
EO	electric organ
EOD	electric organ discharge
f	frequency of spiking within a defined time period
Hz	Hertz, per second
I	Intensity, voltage
ISI	inter-spike interval
K^+	potassium ion
min	minute
mm^2	square millimetres
ms	millisecond
mV	milliVolts

n number of events

nP nucleus praeeminentialis in the metencephalon

NxN *a* matrix of N rows and N columns

° degrees

PC pyramidal cell

P-unit probability sensory neuron, also called P-type

P-value probability of baseline activity given an EOD cycle

s(t) stimulus vector

$s(\tau)$ stimulus train at time τ

$s_{avg}(t)$ spike triggered average

sec second

$s_{random}(t)$ stimulus vector at random times

STA spike triggered average

t time at the observed moment

T time at end at time interval

TS midbrain torus semicircularis

T-unit time-coding sensory neuron, also called T-type

u eigenvector

x stimulus events

ΔV change in voltage modulation

λ eigenvalue

μ V microVolts

τ time at observed spike sequence

Acknowledgements

I would first like to thank my advisor Dr. Leonard Maler whose immense knowledge, patience, support and advice during the course of this work inspired me. His willingness to teach me physics, mathematics and statistical analysis, as well as point me in the right direction to achieve this goal will never be forgotten and I could never thank him enough.

I would also like to thank all the co-workers in the lab for the insightful and thought-provoking conversations: Maurice Chacron, Jason Middleton, Brent Doiron, Anne-Marie Oswald, and Erik Harvey-Girard. I also want to thank Shoshanah Jacobs for helping me keep things in perspective throughout the entire course of the project as well as for "sound advice".

Finally, I want to thank my family and friends for their ongoing support and continued poking me to "git-er done". They helped me maintain my sanity, and to keep things in a worldly perspective. This would not have been possible without them.

You studied Digital Communication Theory.

I studied Biological Communication Theory.

In memory of my father.

It was a real pleasure.

Chapter 1: Introduction

1. The Sensory Experience

All animals require an accurate portrayal of their environment in order to guide their actions in an appropriate manner. Specialised transducers convert various forms of energy (vibration, electromagnetic) or the presence of specific chemicals (e.g. odorants) to neural activity that reaches the animal's nervous system; the nervous system can often respond appropriately within hundreds of milliseconds from the initial sensory experience.

From this perspective, the brain receives input and computes an output. The neural networks involved in sensory processing, mediated by axonal conduction and synaptic transmission, are limited by relatively slow and unreliable electrochemical reactions. Given these constraints, utilising the entire sensory input from many thousands of transducers in a time critical manner would be difficult. Consequently, incoming sensory inputs are compressed to retain essential information and discard information unnecessary for survival. This is an important feature of many sensory systems.

The relevant input needs to be encoded in such a way as to retain the original information required for survival – for example, the information for determining the location, and nature of conspecifics, food and predators. For some sensory transducers (e.g. photoreceptors) the molecular mechanisms that convert light into electrical activity are well known. In other cases, where little is known about the transducers themselves, scientists can treat them as a black box and focus on the relationship between the sensory input and the neuronal output.

1.1 Attributes of Sensory Input and Receptors

There are many types of sensory inputs such as chemical taste or odorants, mechanical pressure, light etc. There are four attributes to any sensory input: modality, intensity, timing and location. Receptors are generally designated by their modality: somatosensory, visual, auditory, olfactory etc. The coding of modality is via labelled lines from stimulus to the brain – for example, any input that comes via the optic nerve is translated as light because the information is tranduced solely to the visual cortex. The intensity of the stimulus is the amplitude, strength of the signal or the total amount of stimulus energy delivered to the receptor over its integration time. The timing of the stimulation is defined by the onset and offset of the receptor response and by how well the response follows the variation of the stimulus. The relative location of spatially arrayed sensory inputs is typically maintained in topographic sensory maps so that activity at a particular region of the map signals the location of the stimulus.

1.2 Neural Coding

Perkel and Bullock (1968), publishing the outcome of a symposium of the Neurosciences Research Program, defined neural coding as: the mapping of external signals / stimuli to neuronal spike trains and the subsequent downstream decoding of these spike trains with a resulting behavioural output. The challenges that accompany this definition have to do with how to determine the encoding transformation as defined by what aspects of the input signal are represented in the output spike train. Because action potentials are all-or-none events, information must therefore be coded solely by the timing or number of spikes. Coding then becomes more complex because both properties of the stimulus and the way the stimulus changes over time must be encoded in the temporal pattern of neural spiking (Mountcastle 1966).

1.3 Current Theories of Coding

Theories of neural coding began with Lord Edgar Adrian in the 1920s when he was studying sensory neurons connected to the stretch receptor in frog muscle and how they "fired" at a particular frequency correlated to the amount of weight applied to the muscle. By graphing the firing rate versus the stimulus magnitude, he noted a strong correlation: the firing rate increases with increasing stimulus strength, and the initial part of the function is approximately linear and saturates at the maximum firing rate of the neuron (Adrian 1932). He concluded that these action potentials, the sensory signalling mechanism conveyed by single sensory axons, could only vary in terms of their frequency or timing; these two possibilities are currently defined as rate or temporal coding respectively.

A. Rate Coding

The relationship between neuronal firing rate and stimulus intensity forms the basis of rate coding. The firing rate is most simply calculated experimentally by counting the number of spikes emitted by the neuron over some finite interval of time (or integration interval) which is substantially longer than the average interspike-interval. The most reasonable choice for the integration interval is half the shortest period over which the stimulus can be approximated as a constant due to the Nyquist frequency limit (i.e. sampling must be at least twice the maximum frequency occurring in the transmitted signal). Since only the total number of spikes is considered within the time-interval, the information contained by the pattern of spikes is discarded (de Ruyter van Steveninck 1988).

Rate coding is suggested to be the method of information transfer at cortical areas of the brain such that the spatial-temporal pattern of feature selectivity were originally determined by reverse correlation methods in various cortical centres like the primary visual cortex (Jones & Palmer 1987, Reid et al. 1991, DeAngelis et al. 1995, Reid & Alonso 1995, Ringach et al. 1997), auditory (deCharms et al. 1998), and somatosensory (DiCarlo & Johnson 1999). In these reports, there is a high degree of variability in the spike rate within a particular time frame when presenting a stimulus many times and this variability is considered noise. Cortical noise is still controversial (deCharms & Zador 2000).

There is no doubt stimulus attributes are encoded in some fashion into a variable rate coding spike train that fluctuates in some manner around a mean spike rate. If the spike number per interval varies between multiple similar stimulus presentations, it is sometimes interpreted as noise (Zohary et al. 1994); the source of this noise will be discussed later. However, it is possible that the firing rate does not describe the entire stimulus as other theoretical encoding schemes (see below) correlate stimulus-response spiking patterns without requiring firing rate. Nonetheless, the rate-coding model requires pre-defined assumptions about the nature of the neural code rather than the preferred method of using the spike train as an exploratory guide for characterising the code.

B. Temporal Coding

A temporal code occurs when the precise timing or patterning of spikes contains significant amounts of information about the stimulus (Theunissen & Miller 1995; Bair and Koch 1996; Berry et al. 1997; Rieke et al. 1997; Mechler et al. 1998; Warzecha et al.

1998; Kreiman et al. 2000). In essence, then the integration interval is equal to the instantaneous moment of a spike's presence. This precise spike timing should reflect the nature of the encoding process and the temporal properties of the stimulus, as in the auditory system regarding speech (Sachs 1984) or echolocation in bats (Wotton 2004). But temporal coding is not relegated to single spikes: spike patterns can code for specific stimulus features such as spike bursting coding for low frequency input (Oswald et al 2004).

It is sometimes suggested that temporal coding occurs only if the stimulus contains precisely timed changes evoking spikes reliably at specific times (Kreiman et al. 2000). However, this is an incorrect assumption because the same stimulus pattern can elicit a strong or weak response depending on the timing of pattern occurrence. Though the precision to which this must be measured has yet to be determined (e.g. milliseconds? nanoseconds?) (Kreiman et al. 2000). Theunissen and Miller (1995) state that the temporal code can only exist if the information carried by a spike is on a time scale shorter than the fastest time scale characterising the variations of the stimulus. The unknown effects of the precision of spike timing on coding is beyond the scope of this thesis.

C. Information Theory

The amount of information, the precision of transmission, and the efficiency of decoding the spike train may depend on the reliability of intervals between temporal impulses (Perkel and Bullock 1968) – defined as the inter-spike interval (ISI). However, information theory is associated with the efficiency and limits of information processing

and studies the correlations between various information-carrying stimuli. While the basic spike generation process in neurons appears to be precise and reliable (Mainen and Sejnowski 1996; de Ruyter van Steveninck et al. 1997; Kreimann et al. 2000), information theory cannot account for the overall variability in spike sequences evoked by repeated presentations of the same stimulus (Abbott and Sejnowski 1999).

Perkel and Bullock's (1968) seminal monograph suggested that instead of a uniform average count of spikes within a fixed window (rate coding), more recent spikes may be given more weight than older ones; in other words, each impulse may have a decaying effect with time – perhaps dependent on the stimulus – on subsequent impulses on post-synaptic neurons. Regardless, the response characteristics of neurons in a number of different systems appear consistent with various coding strategies, as long as a realistic or "natural" stimulus is employed when correlating the character and efficiency of the neural code (Gabbiani and Koch 1996).

D. Inter-neuronal correlations

At the beginning of this section, both temporal and rate coding are mentioned as the only two plausible sources of coding in a neural spike train caused by the variable environmental input. Population coding via correlated or synchronised coding, as well as in the "pattern" of activity across the population, across multiple neurons might increase sensitivity (both accuracy and detection) of unique or low-intensity signals in various uncharacterised ways that may include the synchronous timing of spikes, averaging out neuronal noise, or decreasing the jitter involved in phase coding and other temporal specific coding strategies without signal loss (Singer 1999; Kreiman et al. 2000; Goense

& Ratnam 2003; Benda et al. 2006). By combining the neuronal inputs from numerous sensory afferents, which stimulate regions in the topographically-arranged input regions of the brain in an organisation similar to the skin-surface pattern, it may be possible to see an increase in the probability of object detection.

2. Weakly Electric Fish

When considering what constitutes a model organism for scientific investigations must account for the following factors: ease of accessibility to the system of interest, similarity of the model organism to others, breadth of scientific knowledge on the model organism already available, and cost (purchasing, husbandry, space etc). These factors should be carefully evaluated among the available model organisms before developing a long term project. For the purposes of studying neural sensory coding, these weakly electric fish have easily accessible receptors, relatively simple neurons and central targets; are generally well researched in the area of behaviour and electric sensory systems, and are extremely cost-effective and easy to maintain. In addition, the model neural system is similar to the auditory, vestibular, and even perhaps to some specific cells of the visual system.

Weakly electric fish are nocturnal, leaving their sheltered crevices to enter fast-flowing currents for foraging, and are widely distributed through both tropical freshwater river systems, predominantly in South America and Africa, in addition to marine ecosystems. The species are divided among two major families: the mormyriforme from Africa, and the gymnotiform from South America. Almost all mormyriforme generate pulse-like discharges, as do large numbers of genuses of gymnotiform fish. The electric organ discharge can be pulse or wave-based: pulse-type produces brief broad-spectrum frequency electric discharges followed by relatively long and often highly variable intervals of silence (Bastian 1976, 1977); the wave-type discharges in a quasi-sinusoidal manner with the duration of pulses comparable to the duration of the ISI (Moortgat et al. 1998; Zakon 2002). There are a few wave generator gymnotiform families - Sternopygid,

Eigenmannia, *Apteronotid*. I have chosen to study electroreceptor coding in the wave type weakly electric fish, *Apteronotus leptorhynchus*, because of the large body of work on the role of its electric sense in communication and prey capture.

Weakly electric fish use their electric field as their "eyes and ears" producing a detailed short-range analysis of their surrounding as it pertains to the river bed, plants, food, other fish, and potential predators. The electric field, produced by specialised electric organs (discussed below), do not serve an offensive or defensive role like the strong organs of the electric ray or the electric eel. Neither is the weak electric organ an example of the initial stages of the evolution of such a system, as it falls within a completely different adaptive peak. These electric fish have improved capacities to actively and constantly probe their nocturnal environment, and to exchange information with conspecifics (Kramer 1990). Besides, an organ designed to continuously produce an electric field for electrolocation and communication must be weak: the energy cost of a continuously strong field would be energetically prohibitively too high. In addition, too strong an organ would be counterproductive as it would signal the presence of the generating individual to non-electroreceptive prey and predators.

2.1 General Description and Behaviour of *A. leptorhynchus*

The weakly electric fish *A. leptorhynchus* – commonly referred to as a knifefish - is identified by a striking appearance: a cylindrical, laterally compressed body with an extended snout and jaw, eyes on contralateral sides of the head; a ribbon fin for locomotion moving in an undulating motion that runs the length of the ventral side (anal) from just behind the gills to the tail; and pectoral fins behind the gills to aid in lateral and rotational movements. The electric organ, the source of the electric field or electric organ discharge (EOD), is located in the caudal two thirds of the trunk and runs beside the spinal cord.

In these fast-flowing currents of the river systems where they forage, they must have a sensory reference mechanism relative to the ground or rooted vegetation in order to not be swept away, and a locomotive system to enable these fish to monitor and detect nocturnal migration of prey. As such, *A. leptorhynchus* have a locomotory system that allows them to swim forward, backwards, sideways, and hover. These knifefish have a long ribbon fin that extends the length of the ventral body. By rippling the fin, the fish can generate the force it needs in the forward / reverse direction, and the lateral fins control the roll, sideways movement, and also aid in hovering (Nelson and MacIver 1999). Since the lateral-fin control is independent of the ribbon-fin control, these knifefish have considerable freedom in orientation, and therefore the electroreceptor array and organ, as it moves through water. Given directional flexibility, this mode of swimming provides a high degree of maneuverability and is well suited to foraging in complex environments (Blake 1983) enabling the fish to electrically probe any object of interest.

During swimming, the body is typically rigid to minimize EOD distortions, but this species has the ability to curve their body to focus the EOD. During searching, *Apteronotus* swims with its head pitched at 30° (downwards when moving in the forward direction, and upwards in the reverse direction), with prey detection marked by backwards swimming coupled with a sideways roll, keeping the prey dorsal of the fish while moving closer to the fish's mouth (MacIver & Nelson 2001). Since the majority of tuberous electroreceptors are found on the dorsal surface and on the face (Carr et al. 1982), these probably help the fish to navigate for the final trajectory of prey capture.

During prey capture and detection, these fish swim at approximately 10 cm/sec and their prey move at 2.4 cm/sec. This, in combination with the size of the prey, and rapid changes in velocities during initial detection, produced slow modulations of the EOD amplitude at frequencies typically less than 24 Hz (Nelson and MacIver 1999). From their analysis, these authors conclude these fish can initiate prey capture within ~200ms of initial detection.

2.2 Electroreception – Electrolocation and Electrocommunication

Lissmann (1958) originally observed electroreception when these weakly electric fish demonstrated the ability to distinguish among objects differing only in electrical impedance. The author discovered that this ability was due to the active ongoing EOD and sense organs capable of measuring the local strength of the electrical field at different parts of the fish's body surface. Weakly electric fish like the *Apteronotus* possess both an electric organ and electroreceptors (see below) that encode modulations of the EOD - together they form the active electric sense that is used for active electrolocation: detection of conducting and non-conducting objects via their distortion of the self-generated EOD. The electric sense is also used for electrocommunication in which modulations of the EOD signals the identity, behavioural states and intentions to other nearby conspecifics (Carr and Maler 1986).

Defining electroreception is difficult. This is due to the intimate ties between the physiology and activity, requiring a compound understanding of the physiological components involved in producing, receiving, and ultimately translating the electrical wave into the neural code transduced along the sensory neuron to the brain, along with the behavioural responses to an electric field generated by either specialised organs controlled by brain structures or to naturally occurring external electric fields.

2.2.1 A Definition of Electroreception

A. Electrocommunication

EODs may be useful for communication over distances of several meters depending on the strength of the signal and sensitivity of the receiver (Schleich and Bullock 1974; Lissmann and Machin 1958; von der Emde 1999); *Apteronotus* can detect a stimulus at approximately 21.5cm/mV given the 0.1μV/cm sensitivity. When two fish that produce similar EODs are spatially close to one another, the EODs can combine together to form a complex field. Detection of this complex field can induce unique behavioural responses: either chirping (Bullock 1969) or a jamming avoidance response (Heiligenberg & Partridge 1981). Chirps are brief increases in EOD frequency and decreases in amplitude, lasting ten to a few hundred milliseconds, even up to a few seconds and occurs during social encounters, hierarchal domination, and fighting. Another response characteristic is the jamming avoidance response when the electric fish either raises or lowers their EOD frequency to avoid having EOD "contamination" during prey-detection (Heiligenberg 1980; Bastian 1986).

B. Electrolocation

Electrolocation refers to the detection and property analysis of external objects through electric field distortions. There are two types of electrolocation found in nearly all electric fish: active and passive electrolocation (review Bastian 1986). Passive electrolocation occurs by the surface electroreceptors attuned to naturally occurring surrounding electrical forces (magnetic poles, gravitational etc.). Active electrolocation relies on the analysis of the spatial and temporal patterns of a self-generated

transepidermal potential by an electric organ that is modulated by surrounding objects. This voltage modulation depends on the size, distance, shape and electrical impendence of objects and is used to locate, physically align, and even possibly identify objects. In both active and passive electrolocation, objects with impedances differing from the surrounding water cast "electrical shadows" on the body surface of fish (Bastian 1981; Rasnow 1996; Nelson et al. 1997; Caputi et al 1998; Assad et al 1999; Nelson and MacIver 1999; Nelson 2005; Babineau et al. 2006) and are picked up by the electroreceptors located along the body, face, and snout (Carr et al 1982).

2.2.2 Organ Systems involved in Electroreception

A. Electric Organ

The electric organ is a specialised system of cells derived from either myogenic (muscular) or neurogenic (neural) tissue. Most species of weakly electric fish are myogenic and only the *Apteronotids* are neurogenic. This is important as the EOD is not silenced when using a neuro-muscular inhibitor to immobilize the fish. A neurogenic-derived electric organ contains axons of electromotoneurons called electrocytes whose early development process begins in a myogenic state; in the *Apteronotid*, adult electrocytes are J-shapes electromotoneurons where propagation around the J-loop produces the phases of the EOD (Bennett 1971). These electrocytes are placed end to end down the body along the anterior-posterior body axis. Individual EOD waveforms (discharge type and amplitude) and the frequency of the EOD can be used to identify species, sex, reproductive and social status; the EOD wave-shape and frequency have been shown to change under hormonal control in adult fish (Heiligenberg & Bastian 1984). This inter- and intra-species specific EOD may be the result of differences in several morphological and physiology features of the electric organ: the innervation patterns and coordinated activation of the electrocytes; the size and shape of the electrocytes; the length, position, and number of (longitudinally) arranged electrocytes; and the orientation and position of insulating bands of connective tissue that channel ion flow across the electrocytes membranes (Bennett 1970; Frey & Eichert 1972; Bullock 1982; Caputi et al. 2002; Stoddard 2002; Albert & Crampton 2005)

Individual electrocytes generate approximately 100uV potentials (Bennett 1971; Bass 1986). The voltage and current are affected (similar to batteries) whether

electrocytes are in series or in parallel respectively, manifesting different EOD frequencies and various complex wave shapes (Kramer et al. 1981). It is also the synchronous activity of these electrocytes that ultimately defines the output frequency (Kramer et al. 1981). Regardless, the current generated by the electric organ leaves the fish from the tail (or head) depending on the orientation and electrical properties of electrocytes (Heiligenberg 1977).

For instance, *Apteronotids* have neurogenic electric organs. Over the millennia, it is postulated that presynaptic nerve fibers lost contact with muscle cells and eventually formed the neural based organ. Various species of *Apteronotids* have different discharge waveforms related to organ morphology and physiology, but are all characterised by their high frequency (>600Hz). The high frequency EOD may be due to a command pathway entirely made of electrotonic synapses and specialised anatomy and physiology of the organ (Pappas and Waxman 1972). The electric organ frequency is dependent on temperature (Bullock 1970); yet if the temperature is held constant, the frequency is extremely constant with an overall CV of 0.3% over 10min (Bullock 1969; Moortgat 1998) and probably represents most stable neural pacemaker activity in the animal kingdom. This stability aids in the detection of environmentally derived electro-potential modulations. Despite the relative stability of the EOD, short-term alterations occur in the form of transient frequency or amplitude modulations (by objects or conspecifics in the surrounding environment), both of which will be discussed later.

The phase and amplitude of the electric organ discharge waveform displays a complex spatio-temporal pattern of transepidermal potentials along length of the fish (Assad et al. 1999; Rasnow 1996). The EOD waveform is not constant along the length

of the body (Bennett 1971; Hoshimiya et al, 1980). The current produces a 3-D gradient of voltage in the water that the animal can detect, however it is useful only within 1-2 body lengths of fish (see Electrolocation). However, even when object is close, the change in voltage magnitude (ΔV) is only a small fraction of local EOD measured with no object present (Chen et al. 2005, Babineau et al. 2006; Rasnow 1996).

B. Electroreceptors

The specialised cutaneous receptors responding to the current flow across the skin are called electroreceptors which are believed to be evolutionarily originated from the inner hair cell type receptors as are the receptors of the lateral line. There are two major classes of electroreceptors: tuberous electroreceptor organs detect the self-generated electric field while ampullary electroreceptor organs detect external electric fields. The related mechanosensory lateral line, found in almost all fish and some amphibians, detect movement and vibration in the surrounding water, help avoid collisions, and help orient the fish in relation to water currents (Popper and Platt 1993). All three systems provide information to the individual for the purpose of hunting and spatial orientation (Hoekstra and Janssen 1986).

All electroreceptors have a similar biophysical makeup (Zakon 1984) with unique structural and functional properties of the receptor cells. The receptor cell contacts the afferent nerve fibre by chemical synapse with a presynaptic ribbon (Kramer 1990). The afferent nerve responds to weak stimulus voltage modulations. Ohm's law states that current flowing inward across the (passive) resistance of the luminal membrane will produce an internal-negative voltage change (ΔV) across the basal or synaptic membrane.

Therefore, the luminal membrane hyperpolarises and the basal membrane depolarises with the current flow across the receptor and skin. Since electroreceptors are primary sense receptors and do not produce action potentials; depolarisations of the basal synaptic membrane increases the probability of opening voltage-gated Ca^{2+} channels at the synapse, which increases the probability of release of the excitatory transmitter, glutamate (Bennett 1971; Bennett and Obara 1986; Zakon 1984; Moller 1995). This in turn depolarises the postsynaptic nerve fibre and increases the probability of its emitting a spike.

Ampullary receptors – Physiology and Function

A. leptorhynchus – the model for this study – have ampullary receptors supporting a supplementary role for afferent input (Bastian 1986a,b). Ampullary electroreceptors detect exogenous electric fields with frequencies of 0.1-50 Hz (Bennett 1971b; Zakon 1984), therefore coding the low frequency signals generated by most aquatic animals. By plotting the frequency of the neural discharge versus the amplitude of the low-frequency voltage stimulus applied to the canal opening of the ampullary receptor, the discharge frequency forms an S-curve response that silences at a particular voltage and "saturates" at approximately double the baseline frequency (Bennett 1968). Since the density of ampullary organs is greatest on the head and decreases toward the tail, it provides the greatest resolution for the final prey approach. However, as these are not the focus of this study, a more detailed explanation about the response as well as the physiology of the receptor will not be described further.

Tuberous Receptors - Physiology

Tuberous electroreceptors are the main sensory receptors involved in exploring the surrounding environment for these weakly electric fish, and communication with other conspecifics (for review: Bullock 1982). These receptors respond to the increasing and decreasing EOD modulations caused by the interaction with conducting and insulating objects respectively.

To understand the uneven distribution of the approximately 13,000 to 17,000 tuberous receptors on the skin surface of *Apteronotus*, divided up with approximately 20-25 / mm^2 on the snout, 15 / mm^2 on the head and about 3 / mm^2 on the body (Carr and Maler 1982), involves understanding the behaviour of these fish because evolution has allocated the distribution to maximise prey detection likelihood. Initial detection is over greater distances covering large swaths of the body that, if the stimulation is of interest, is used again for a second pass while reversing. As the fish brings the prey closer to its face, mouth and snout, the speed slows and the distance between the predator and prey decreases, requiring a higher density of receptors to retain the same spatial resolution (MacIver and Nelson 2001). The receptor density is approximately the same across various different fish species. (*Apteronotus* Carr et al. 1982; *Gymnotids* Caputi et al. 2002; *Eigenmannia* Bastian 1981a, b).

The physiology of tuberous receptors is unique. Unlike the ampullary receptor whose receptor channel is filled with water connecting it to the environment, the tuberous receptor has a short canal from the skin surface filled with mucus connecting the outside water to a chamber containing 20-40 receptor cells (Zakon 1984; for *Sternarchus* Bennett 1989). However, the receptors cells are not directly connected to the mucus. Instead an epidermal layer loosely covers the apical surface of the receptor cells. The reason for the

mucal and epidermal layer structure is unknown. In addition, these receptor cells lack the cilial structure on the apical surface of the ampullary receptors but contain a large number of deep, microvilli-covered invaginations (Bullock et al. 1975) increasing the surface area of the luminal membrane, which decreases the resistance facilitating the detection of smaller changes in voltage across the receptor cell (Ohm's Law) due to this increased sensitivity. Each receptor cell contains a number of synaptic ribbons on the epidermal basement membrane transducing the signals through 16 synaptic contacts onto a single innervating axon (Bennett 1989). With upwards of 40 receptors cells, each tuberous electroreceptor has >640 connections onto the single axon of the sensory afferent.

These tuberous receptors have been shown to be generally tuned to the near peak power frequencies of the fish's own EOD or of their conspecifics (Hopkins 1976). There are several mechanisms contributing to band-pass tuning: the shunting of high frequencies across the electroreceptor canal and chamber is minimised by the thin layers of epithelial cells presenting a low capacitance; the protruding apical face comprises of a highly proliferated cell membrane serving as a series blocking capacitor to assure only voltage changes not slow relative to membrane time; and the basal face has an active conductance (K^+ and Ca^{2+}) (Zakon 1984). The synaptic connections of the afferent fiber specialisations are diverse but typically reflect a convergence from a single chamber of multiple receptors onto a single afferent fiber with a large number of ribbon synapses.

Tuberous Receptors - Function (i.e. T-units and P-units)

There are two types of electroreceptors: T-type (or T-units for time coders) and the P-type (also called P-units for probability coders) (Scheich et al. 1973). T-unit afferents are phase-locked (each EOD cycle generates one action potential) and frequency-locked (continuously spiking at same frequency in time-locked fashion) at an extremely high precision with the animal's own EOD (Bullock and Chichibu 1965). Therefore the time-coding pathway marks the time and phase of each EOD with high reliability, and it has been postulated that T-units phase shift during in response to amplitude modulations of the EOD during communication to detect the interacting electrical discharges of other fish (Scheich and Bullock 1974). In *Apteronotids*, there are very few T type electroreceptors as the interval between EODs is so short and the temporal intervals available for phase coding are often less than 1ms. I did not examine the coding properties of T units for my thesis and will not discuss them any further.

Unlike the T-type electroreceptor, P-type electroreceptor afferents discharge spontaneously on the upward phase of the baseline EOD oscillation (phase-locking) in a probabilistic manner of less than one spike – or action potential – per cycle (Scheich et al. 1973; Scheich and Bullock 1974; Viancour 1979; Bastian and Heiligenberg 1980). The probability (P-value) is the ratio of the number of spikes per second to the frequency of the EOD, and the probability across the population of P-unit afferent neurons range from 0.1 to 0.5 (Bastian 1981; Xu et al. 1994; Wessel et al. 1996; Xu et al. 1996; Nelson et al. 1997; Ratnam and Nelson 2000; Kreiman 2000; Chacron et al. 2001; Chacron 2005; Ludtke and Nelson 2006). The distribution of the spontaneous activity of P-values for the P-unit afferents has never been physiologically / anatomically explained. Chacron et al.

(2001) proposed that a probabilistic number of synaptic sites stimulate the afferent neuron with every EOD cycle, and that the number of actives sites at one receptor is uncorrelated with the number of actives sites at another receptor for the same EOD cycle.

This spontaneous activity, or background afferent frequency, is the carrier for the signals- amplitude modulations of the EOD caused by the presence of objects or communication signals; yet without a modulated input, the carrier transmits no information (Perkel and Bullock 1968). When the EOD amplitude is modulated, the spike train adapts to the signal intensity, tracking a low frequency stimulus with a high level of accuracy (Benda et al. 2005). However, if the stimulus persists for a length of time without change, the apparent intensity diminishes and the spike rate slowly reverts to a new baseline related to the stimulus intensity (Benda and Herz 2003; Benda 2005).

The high level of accuracy of amplitude tracking by P-units mentioned in the previous paragraph has been studied and modeled extensively (Bastian 1981a; Wessel et al. 1996; Xu et al. 1996; Nelson et al. 1997; Ratnam and Nelson 2000; Kreiman et al. 2000; Chacron et al. 2001; Benda and Herz 2003; Benda et al. 2005; Chacron et al. 2005a; Ludtke and Nelson 2006). While the exact mechanism by which the tuberous receptor converts external voltage modulated signals into action potentials is unknown, previous studies have used indirect methods to demonstrate a correlation between the external voltage signal and the spike trains of P units.

C. From Receptor to Brain

The physiological specialisations of receptors are established in the sense organs where information selection for phase and amplitude, or time and/or intensity, occurs. The two electroreceptive sensory cells (P and T units) constitute starting points of separate anatomical pathways (Carr et al. 1982; Heiligenberg and Dye 1982) which are subsequently divided again by the central nervous system pathways to enhance and refine detection. The convergence of these afferent inputs from multiple receptors onto higher level cells increases the spatial resolution and reduces time-encoding jitter (Wessel et al, 1996; Kreiman et al 2000; Goense & Ratnam 2003).

The P-unit afferents both excite and inhibit the two principal electrosensory lateral line lobe (or ELL) efferent neurons: the basilar and non-basilar (or superficial) pyramidal cells (Maler 1979; Maler et al 1981; Saunder and Bastian 1984; Heiligenberg and Partridge 1981) which are also called E and I cells since these cells react to increased EOD amplitude with excitation and inhibition respectively. These are further subdivided into deep, intermediate and superficial depending on their depth in the cellular layer. Non-basilar pyramidal cells have short basal dendrites, large apical dendrite arbors and low-frequency firing rates whereas basilar (especially deep basilar) pyramidal cells have small apical dendrite arbors, long basal dendrites, and higher frequency firing rates. As a whole, the ELL is a collection of neurons and circuits sensitive to the rise and fall of EOD amplitude (Saunders and Bastian 1984; Shumway and Maler 1989).

The ELL is divided up into four segments: the medial segment receives input from ampullary afferents only, and the other three segments of the ELL (centrolateral, centromedial, and lateral) receive input from both P and T units which terminate on four

distinct cell types and form identical somatotopical maps (Heiligenberg and Dye 1982; Kramer 1990). These four segments of the ELL have ascending efferent projections transmitting topographically ordered electrosensory information to the midbrain torus semicircularis (TS) and the nucleus praeeminentialis (nP, metencephalon) (Heiligenberg and Rose 1985; Shumway and Maler 1989; Berman and Maler 1999; Maler 2007). Within the TS phase and amplitude pathways converge onto neurons selective for four different combinations of amplitude and phase: amplitude fall-phase advance, amplitude rise-phase delay, amplitude fall-phase delay, and amplitude rise-phase advance (Heiligenberg 1991).

The TS is the main site of electrosensory processing responsible for combining the phase and amplitude information in order to perform the necessary calculations for electrolocation and communication. The TS is a large, laminated midbrain structure equivalent to the inferior colliculus in mammals: 12-15 laminae and 48 cell types (Carr and Maler 1981, 1986; Scheich and Ebbesson 1981). The dorsal TS is responsible for the extensive processing required from electrosensory information (the ventral torus manages the auditory and mechanoreceptive sensory systems). This higher electrosensory center also transmits synaptic input back to the ELL (Sas and Maler 1983, 1987) to modulate, inhibit, and amplify important stimulus features (Bastian 1986a,b; Bastian 1999; Berman and Maler 1999). An example is the modeling of the jamming avoidance response (Bullock et al. 1972; Carr and Maler 1985). The IV, VI, and VIIID laminae of the dorsal torus must have strong connections to allow for active real-time comparisons of information from various sides of the body surface to determine spatial orientation. However, this research study does not extend into this area of analysis.

3. Analyzing Electrolocation Properties

An accurate representation of the statistically variable structure of the incoming signals (Attneave 1954; Barlow 1961) is required to have an efficient stimulus-response coding strategy in which the electric field correlates effectively to the neural output. Determining the correlation between stimulus and the resulting neural spike train can be performed in various ways. While using naturally-produced signals to probe this relationship is ideal, sometimes it is inefficient especially if the source is the prey itself: the uncontrollable variability, interactive effects between environment and subject, unknown (or subtle) properties of the stimulus, and difficulty in controlling the location of the signal. As such other methods to stimulate electroreceptors have had to be employed including using spheres of various conductances (Bastian 1981a) or tones of various frequencies and combining their effect (Scheich 1977; Bastian 1981a; Arnegard et al. 2006); and even representing other conspecifics (Benda et al. 2005, 2006).

3.1 Stimulation

As mentioned before, electrolocation is limited to very short ranges: the change in the transepidermal voltage is negatively proportional to the cube of the object's distance - the object must increase nine-fold in diameter to compensate for three-times the distance (Bastian 1986; Chen et al. 2005; Babineau et al 2006). The farther away the object, the more "blurred" the electric shadow becomes on the fish's body and perhaps the ratio of the magnitude to the "blurriness" is used as an object cue (von der Emde et al. 1998; Lewis & Maler 2001). This transepidermal perturbation is perpendicular to the component of the electric field directed from the object, thus is largest where the electric field component is greatest (Rasnow 1996).

Before using electrical stimulation tools, experimental modalities were produced via conductive and non-conductive objects (spheres, squares etc) of different sizes and shapes at various distances and velocities to influence the time-course across the surface of the animal's skin and ultimately represented the size of the amplitude modulations (AMs) affecting P unit firing (recent papers include Assad et al. 1999; Babineau et al. 2006; Chen et al. 2005). Eventually, this was changed to the digital/analog stimulation devices and stimulation patterns like step pulses or single amplitude and frequency "tones", single frequency (i.e. sine wave) amplitude modulated signals (SAMs), and random frequency amplitude modulated signals (RAMs). The step function is an instantaneous change in amplitude of the signal (or step) to a constant intensity held for a particular length of time, and then released. This intensity change (either up or down) at very high frequencies results in rapid adaptation of the P unit response (Benda et al. 2005). Amplitude modulation signal generation - be it sinusoidal amplitude modulation

(SAMs) or random amplitude modulation (RAMs) of the carrier EOD – are more natural stimulus patterns that avoid excessive adaptation.

Matching the neural performance to the global statistical properties of natural signals was proposed by Attneave (1954), and dynamic RAM stimuli are the closest to achieving this type of stimulus-response relationship without using actual high-quality recorded sounds from their natural environment. This was utilized by Brenner and Bialek (2000) as "white noise" in a frequency range expected to be encountered by the fly. This study will follow this same reasoning using both low frequency RAMs (Gaussian noise from 0-4 Hz) as a stimulus and extracted the f-I curves from 32 ms of the evoked spike train and higher frequency RAMs (gaussian noise from 0-50Hz) and extracting pre-spike stimuli for covariance analysis.

3.2. Statistical Methodology and Previous Results

The goal in any statistical analysis of stimulus evoked spike trains is to match the neural performance to the global statistical properties of the natural signals that induced the response. This also presupposes responses are matched to the average signal in real time and are sensitive to amplitude fluctuations around the mean (Ruderman and Bialek 1994). These analyses can be performed on recordings of both stimulated and baseline conditions.

Simple indicators such as the mean and variance of the number of spikes recorded during these time windows provide universal and effective ways to quantify conditional responses (Parker and Newsome 1998). In fact, the variance-to-mean ratio of increasing time intervals (or Fano Factor) can indicate how the stimulus-response relationship changes: a decreasing slope indicates correlated spikes (via auto correlated spike trains; Ratnam and Nelson 2000) such that the variance does not increase as quickly as the mean.

A. Frequency-Intensity (f-I) Curves

Bastian (1981a) noted that the amplitude and frequency characteristics of the EOD modulations must be compared with the receptor's responsiveness to the signal in order to determine what type of information the receptors transmit to the CNS. The initial use of sinusoidal AMs and conductive spheres indicated a very strong linear relationship of mean spiking rate to mean signal amplitude (Bastian 1981a; Zakon 1986; Wessel et al. 1996; Nelson et al. 1997). This observation of this relationship used an analysis technique formulated originally by Adrian (1932): temporal summation of the input and output over

a predetermined time window. This sampling time interval is calculated by the Nyquist frequency.

It is suggested that at sufficiently large amplitudes (>10mV/cm, or ~500% of the EOD peak-to-peak amplitude), the electroreceptor afferents phase-lock 1:1 and fire once for each cycle of the sinusoidal electric field (Hopkins 1976; Wessel et al. 1996). And all this transmitted information depends on the mean firing rate of the afferents, the cut-off frequency and contrast of the stimulus (Bastian 1981a). But these stimulation analyses associate a correlation of stimulus intensity to the firing rate and do not consider the impact of the preceding spike or stimulus sequence.

This sequence might include any number of prior spikes; the fact that the strong (negative) correlation of baseline interspike intervals (ISIs) only extends across two ISIs (Chacron et al. 2001) suggests that only short sequences contain such intrinsic correlations. The negative correlations between ISIs indicate a tendency for long ISIs to be followed by short ISIs (and vice versa), which can reduce spike count variability and thus cause the decrease in the Fano factor with counting window duration (Chacron et al. 2001). The negative ISI correlations are not likely to have a major impact on the f-I curve since there were typically many ISIs with this time window.

B. Stimulus Reconstruction

As mentioned above, by modifying the stimulus to get a particular response the final result is constrained. It is the interpretation of the spiking-sequence response as attributable to a certain stimuli that makes this method a powerful analytical tool. The stimulus must be a RAM, frequency-constrained "white noise" stimulus from which short waveform sequences preceding a particular spiking sequence are considered representative of a "cause-effect" event. This spiking sequence could be one spike, a certain number of spikes within defined time frame, or even any number of inter-spike intervals.

Following Brenner and Bialek's (2000) original modeling assumptions, the spike rate for *A. leptorhynchus* has been shown to be dependent on stimulus amplitude; while particular frequency bands have been associated with prey detection and communication, the frequency ranges used in this experiment (0-50Hz) are well within the acceptable limits of prey-detection (Chacron et al. 2001). By averaging these spike sequence-dependent short-waveform sequences, we can obtain the conditional mean waveform (known as reverse correlation or spike-triggered average STA stimulus) (De Boer and Kuyper 1968; Wessel et al. 1996; Rieke et al. 1997). Previous investigations using stimulus reconstruction techniques showed that tuberous electroreceptor afferents performed well – spikes triggered by a large positive slope encoded 40-80% of the information about stimulus time course (Wessel et al. 1996; Metzner et al. 1998; Kreiman et al. 2000).

C. Covariance Analysis Method

Stimulus reconstruction techniques, which average all pre-spike stimulus waveforms, do not consider variability or multi-dimensional effects such as the change of the stimulus as a cause for spike generation. Instead, by calculating the covariance matrix of the pre-spike stimulus (de Ruyter van Steveninck and Bialek 1988; Brenner et al. 2000; Slee et al. 2005; Fairhall et al. 2006), one can extract multi-dimensional aspects surrounding the stimulus-response relationship.

If we assume that the stimulus vector $s(t)$ defines the stimulus prior to an observed spiking-sequence, where t is defined as the time interval from 0, the observed moment, to end at time interval T; and the set of stimulus vectors for all observed spike sequences is $\{s_x(t)\}_{x=1..n} = \{s_1(t), s_2(t), \ldots, s_n(t)\}$; then the STA stimulus is calculated by $s_{avg}(t) = \Sigma_1^n s_x(t)/n$, for each time point $t = 0 \ldots T$.

Averaging smoothes out details of $\{s_x(t)\}$; it is an assumption that only one component of the stimulus was responsible for the spiking sequence to occur. Perhaps the neuronal spiking sequence encodes not just the amplitude of the stimulus (as calculated by the reverse correlation) but the reliability that a particular stimulus waveform would cause the pre-determined spiking sequence given the same set of stimulus vectors $\{s_x(t)\}$. This probability is similar to computing the covariance matrix, C_{spike}, of the fluctuations around the average (Brenner & Bialek 2000) as C compares each stimulus time-point with every other stimulus time-point and outputs a measure of similarity (see equation 1): a positive covariance means the two stimulus vector time-points generally move together, a negative covariance suggests they are inversely related.

$$C_{spike}(\tau, \tau') = \langle s(\tau) \bullet s(\tau') \rangle - [\langle s(\tau) \rangle \langle s(\tau') \rangle] \qquad \textit{Equation 1}$$

where τ and τ' are measures of time between the observed spike sequence and the end of the time interval. This covariance matrix represents a response ensemble governed by a multi-dimensional Gaussian distribution centered on the mean stimulus waveform (de Ruyter van Steveninck 1988); but it also contains the possibility of random effects of the stimulus. As such, collect the same number of events as spiking-sequences of the same time length, but randomly pick time points along the entire stimulus. Calculate the covariance matrix C_{random} as performed in equation (1) and subtract this from C_{spike}. As a note, though, the average of $\{s_{random}(t)\}$ should be fairly flat – otherwise there is a bias in the selection of the pre-stimulus random points.

The covariance matrix can in turn be reduced to eigenvectors – or perpendicular vectors each describing the stimulus - and a strength measure of the eigenvector called the eigenvalue. The linear vector space is a collection of vectors that translate an *NxN* matrix into single unique values associated with the vector. The calculation:

$$A\lambda = u\lambda \qquad \textit{Equation 2}$$

where *A* is the *NxN* matrix, *u* is a real number (because covariance matrices are symmetric), and λ is an Nx1 vector. There are a total of *N* results to this equation, with sometimes similar *u*'s but different λ. Each λ and *u* pairing are calling eigenvector and its eigenvalue. The (scaled, or percent of sum) eigenvalue determines the magnitude of the response vector within the linear vector space spanned by a basis of the eigenvectors. The largest eigenvalue – in other neural systems (Brenner & Bialek 2000) – have been found to be the equivalent to the spike-triggered average of the stimulus, and the second eigenvalue is its derivative. This is not surprising since both the magnitude of a signal

and its rate of change might be expected to be important in triggering spikes.

Eigenvectors are then projected onto the spike train to reconstruct the original stimulus.

4. Objectives

As mentioned above, the electric field stimulates cutaneous electroreceptors (P-units) that fire probabilistically in phase with the EOD whose probability (P) of discharge ranges from 0.1 to 0.5 (typically 100 - 500 spikes/sec) (Xu et al 1996). However, the majority of papers characterizing the stimulus-response relationship focus on average P-unit responses (Scheich et al 1973, Wessel et al 1996; Xu et al 1996; Kreiman et al 2000; Ratnam & Nelson 2000; Benda et al. 2005) rather than analyzing how each individual neurons encodes the stimulus. The prevailing assumptions are that all neurons function similarly to the response and that baseline activities are irrelevant to stimulus encoding. As such, comparing individual baseline activities to their responses to an external stimulus has been largely ignored. As noted in figure 1A and 1B, there is a distribution of baseline firing rates encompassing frequencies from ~75 to 500Hz (p-values from 0.08 to 0.5). The purpose of this thesis is to determine whether a relationship exists between the baseline firing rate and several known neural coding functional analyses, and if one does exist to describe why the relationship could be useful from a behavioural standpoint.

Chapter 2: Manuscript – Published in Journal of Neurophysiology, 2007

Limits of Linear Rate Coding of Dynamic Stimuli by Electroreceptor Afferents
Daniel Gussin, Jan Benda, Leonard Maler
Journal of Neurophysiology, 97: 2917–2929, 2007.

Introduction

Sensory signals are typically encoded by the patterns of spikes in a population of afferent fibers. Discovering the neural code for a sensory system requires both specifying a map between external signals and the resulting spike trains, and demonstrating that downstream neural circuits can interpret or decode this mapping and therefore direct behavioural output (Perkel and Bullock 1968). The original suggestion by Lord Adrian (Adrian 1932) that the intensity of a stimulus is linearly encoded by the spike rate over a fairly long time window (rate coding) has dominated this field. For slowly changing signals this code can be simply estimated by presenting constant stimuli of varying intensity and counting the spikes emitted over many seconds; this results in a simple spike frequency-intensity (f-I) curve that summarizes the putative code. The advantage of this encoding scheme is that decoding merely requires temporal summation of input over a time window set by the synaptic and postsynaptic membrane time constants. However, this method of estimating stimulus encoding fails for dynamic signals and for neurons with time dependent conductance (e.g. adapting currents). More sophisticated methods such as the use of the spike triggered stimulus average (STA) to estimate the reverse correlation of signal and spike train response have also been employed to estimate the linear encoding of signals (Chacron et al. 2005a; Metzner et al. 1998; Wessel et al. 1996). However, there is typically no obvious decoding mechanism implied by these techniques.

In this paper we analyze encoding and detection in the electrosensory system of the weakly electric fish, *Apteronotus leptorhynchus*. These fish emit a continuous quasi-sinusoidal electric organ discharge (EOD); the species EOD frequency ranges from ~600-1000 Hz and the amplitude varies with fish size, but the EOD of an individual fish has nearly constant amplitude and frequency (Moortgat et al. 1998). The electric field induced by the EOD is sensed by specialised cutaneous tuberous electroreceptors. The most abundant tuberous receptor is the P-unit and it discharges in a probabilistic manner to the upward phase of the baseline EOD oscillation. An important parameter characterizing P-units is their P value, defined as the probability of P-unit spiking per EOD cycle and estimated as the ratio of P-unit frequency to EOD frequency; P values typically range from about 0.10 - 0.50 (P value = 0.10 - 0.60: Bastian 1981a; Xu et al. 1996; Xu et al. 1994). The amplitude of the EOD can be modulated by both the presence of nearby objects (electrolocation) or the EOD of conspecifics (electrocommunication) (Bastian 1981a; Benda et al. 2005; Benda et al. 2006; Nelson 2005; Nelson et al. 1997); electrolocation induces low frequency amplitude modulations (AMs) (typically <20 Hz Bastian 1981a; Nelson and MacIver 1999) while electrocommunication AMs can exceed 200 Hz (Bastian et al. 2001; Benda et al. 2006). These AMs of the baseline EOD are the dynamic sensory signals for the electrosensory system and cause the P-unit firing rate to vary proportionally. P-units have been thoroughly studied and modeled by many investigators (Bastian 1981a; Benda and Herz 2003; Benda et al. 2005; Chacron et al. 2001; Chacron et al. 2005a; Kreiman et al. 2000; Ludtke and Nelson 2006; Nelson et al. 1997; Ratnam and Nelson 2000; Wessel et al. 1996; Xu et al. 1996); P-units are rapidly adapting (Benda et al. 2005; Xu et al. 1996) and are typically studied using sinusoidal

(SAMs) or random AMs (RAMs). The emerging consensus from these studies is that, over the natural range of AM intensities and frequencies, P-units are linear encoders and can predict up to 80% of the AM. However, the reverse correlation and coherence methods often used in these studies again do not point to obvious decoding strategies.

In this paper we estimate the f-I curves of P units using techniques recently developed by Brenner et al. (Brenner et al. 2000). Classic f-I curves were constructed using low frequency noise; these results lead to a simple model of linear encoding with additive noise. The noise appeared to be due to both the well documented variability of baseline P-unit discharge and the sensitivity of P-units to the stimulus slope as well as its intensity. Although it is easy to envision the decoding of this response, our calculations show that the estimated noise levels would preclude the model from detecting weak electrosensory signals. High frequency noise signals and the covariance method were also used to construct f-I curves. We found that P-units responded to a linear combination of time-weighted averages of the signal intensity and its slope; these two variables accounted for almost all the P-unit response variability and the first feature (intensity) contributes most to the response. We conclude that the apparent noise in the response to the signal's intensity (classic f-I curve) is due, in part, to the variation of the signal slope. We suggest a mechanism such that, if the fish were able to decompose the P-unit response into its intensity and slope components, then it could then detect the very weak signals to which it is behaviourally responsive.

Materials and Methods

This study used data from single unit nerve recordings from adult gymnotiform weakly electric fish *Apteronotus leptorhynchus* (10-14 cm). Animals were housed in groups of 3-10 in 150 L tanks, and the temperature maintained at ~28°C. A dose of 100 ppm MS-222 (tricaine methanosulfonate, Sigma, St Louis, MO) anesthetised the fish before surgical and experimental procedures; the fish were then immobilised with an intramuscular injection of Pancuronium Bromide (Sigma) and placed in a water tank (46.5cm x 41cm x 18.5cm) kept at 28°C, and respirated with a constant flow of oxygenated water. The resistivity of the water was typically set at ~4.5 kΩ/cm to match that of the fish's home tank. All experimental protocols were approved by the University of Ottawa Animal Care Committee.

Experimental procedures were as previously reported (Benda et al. 2005). The posterior branch of the anterior lateral line ganglion (innervating trunk electroreceptors) was exposed and glass micropipettes (90-115 MΩ) advanced through the nerve with a piezoelectric microdrive (Inchworm IW-711, Burleigh, Fishers, NY). Action potentials were recorded (Axoprobe 1A; Axon Instruments, Union City, CA), band-pass filtered (0.3-7kHz: PC1; TDT, Alachua, FL), and notch filtered at the fish's EOD frequency (Ultra-Q Pro; Behringer, Willich, Germany).

Two vertical carbon rods (11 cm long, 8 mm diameter) recorded the unperturbed EOD between the head and tail of the fish. Stimuli (see below) were attenuated (PA4; TDT, Alachua, FL), isolated (Model 2002; A-M Systems, Carlsborg, WA) and, for global stimulation, delivered by two stimulation electrodes (30 cm long, 8 mm diameter carbon rods) parallel to its longitudinal axis and placed 15 cm on either side of the fish. All

stimuli were generated by multiplying the fish's EOD (MT3; TDT, Alachua, FL) on a cycle-by-cycle basis with the RAM stimulus; its contrast was controlled via a programmable attenuator.

Local stimulation by 20 Hz sine waves was delivered by two stimulation electrodes (0.005" diameter, 99.95% tungsten wire, California Fine Wire, Grover Beach, CA) 4 mm apart, parallel to the fish's longitudinal axis, and placed within 1 cm of the fish's surface; a 20% contrast was used as above. These local stimulation electrodes had their position adjusted to produce a maximal response from the receptor and we assumed that this identified its location. During both global and local stimulation, two chloridised silver wires insulated up to their tips with nail polish and 4 mm apart recorded the field gradient adjacent to the animals' skin. These silver wires were oriented perpendicular to the global stimulation electrodes at the site of maximal response to local stimulation and thus measured the stimulus delivered to the recorded P-unit. The EOD and field gradient were amplified and low pass filtered (5 kHz; 2015F, Intronix, Bolton, Ontario).

After the P-unit location had been identified (with 20 Hz sine wave stimulation), we used random amplitude modulations (RAM stimuli) to characterize the relationship between the stimulus intensity and P-unit discharge rate (f-I relation).

P-type units were identified on the basis of their phase locking to the EOD, their skipping response to the baseline EOD, and phase locking to direct stimulation. Once a receptor was tested for phase locking to a global 20 Hz AM stimulus, the same 20 Hz AM stimulus was delivered locally to find the receptor on the surface of the fish. By adjusting the position of these local stimulation electrodes along the head-tail and dorsal-ventral axes of the fish, it was possible to find the location producing a maximal response

from the recorded P-unit. The local electrodes used to measure the field gradient at the receptor pore were oriented perpendicular to the global stimulation electrodes but, since the fish's body curves appreciably at its dorsal aspect, were not necessarily perpendicular to the skin. Since the effective stimulus for an electroreceptor is the current flow across it (perpendicular to the skin, Nelson et al. 1997), a correction factor was applied based on measurements of the body curvature; this produced the final estimate of the effective intensity of the stimulus driving the P-unit (average correction: 0.84 ± 0.17 x measured amplitude).

Action potentials, the EOD, the field gradient, and the attenuated stimulus were digitised at 20 kHz with a 12-bit Multi-IO-board (PCI-MIO-16E-4; National Instruments, Austin, TX) on an Intel Pentium IV 1.8 GHz Linux PC. Spike and EOD detection, stimulus generation and attenuation, and pre-analysis of the data were performed online during the experiment with our custom software (Online Electrophysiology Laboratory, created by Jan Benda). All data analysis was performed with MATLAB (The Mathworks, Natick, Ma.).

Estimating the P-unit frequency-intensity (f-I) function.

The classic method for constructing f-I curves calculates spike rates in response to step changes in stimulus intensity. The rapid adaptation of P-units to steady state changes in EOD (Bastian 1981a; Benda et al. 2005; Xu et al. 1996) amplitude precludes this method. Instead we computed f-I curves using two methods adapted from Brenner et al. (Brenner et al. 2000) using double the cut-off frequencies found during late (~2 Hz) and early (~25 Hz) phases of prey detection (Nelson and MacIver 1999): a Gaussian RAM

with a low frequency cut-off of 4 Hz and a contrast of 5, 10 and 15%. Gaussian RAMs with a 50 Hz cut-off frequency were presented for 180s at 10% contrast. The former stimulus protocol was repeatedly delivered for 10s with 2s rests (frozen noise, 15-100 presentations), and analysed using counting windows (32 or 64 ms) to generate the spiking rate versus intensity relationship. The latter protocol, analysed using the covariance method (Brenner et al. 2000), utilised a cut-off frequency that did not exceed the Nyquist frequency for any P-unit in our sample (minimum P-unit mean firing rate can be ~100 Hz), which evoked only one or a small number of spikes over the time scale of the fastest fluctuations in the stimulus; further, a 10% contrast stimuli tests for the full coding range up to saturation of the response. Preliminary experiments had shown that the covariance method works best under these conditions and is not optimal for the 4 Hz cut-off stimulus. P-units, because of their high discharge rate, responded throughout the low frequency stimulus (Fig. 1) and this resulted in gradually decreasing eigenvalues instead of two dominant ones (see below); in this case the covariance method is not informative.

Data analysis - P-unit Baseline Activity.

We routinely computed the interspike interval (ISI) histogram, spike train serial correlations and the Fano factor as previously described (Chacron et al. 2001; Ratnam and Nelson 2000). The Fano factor is the variance to mean ratio of the spike count as a function of the counting interval; we used intervals ranging from 2-1200 ms (absolute time) or 2-1200 EOD cycles.

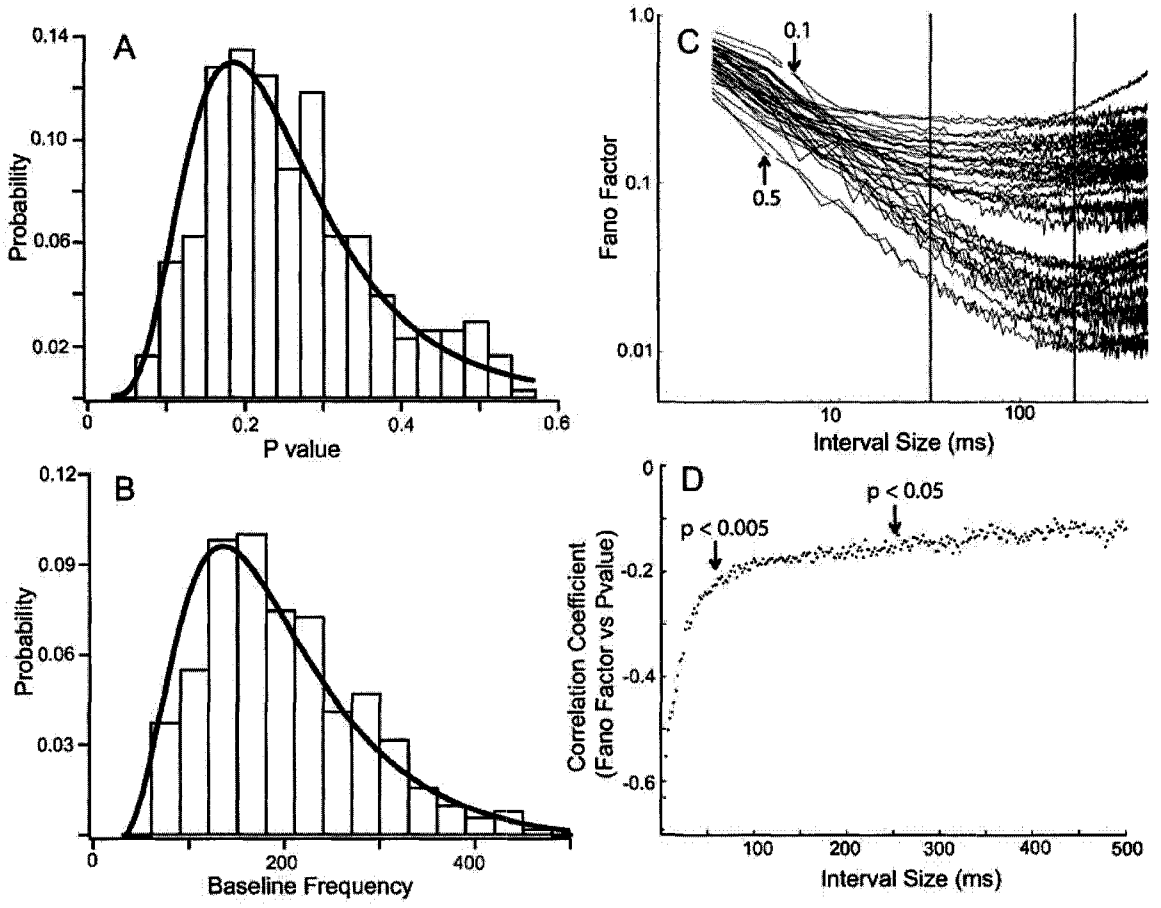

Figure 1: A. The P value distribution and lognormal fit. The μ and σ values are -1.42 and 0.46 respectively with a mean of 0.26 ± 0.11. B. The distribution of P-unit firing rates distribution and lognormal fit. The μ and σ values are 5.23 and 0.44 respectively and a mean of 199 ± 81Hz. C. Fano Factor curves of a subset of P-units. The two vertical lines indicate the 32 ms and 200 ms time points. The arrows identify the P values for two representative units that demonstrate the lower variance of the high frequency P-units. D. Correlation coefficient of the P-value vs Fano factor for varying counting windows, plotted against the corresponding counting windows. With time intervals less than 50 ms, there is a very strong inverse correlation between P value and the Fano factor ($P < 0.005$). Significant negative correlations persist for counting windows up to 250 ms.

Data Analysis - Low Frequency Stimulation

A stimulus with a maximum frequency of 4 Hz could, in principle, be sampled at 8 Hz; in practice, such sampling produced noisy f-I curves. We present analysis using 32 ms sampling bins; sampling at 64 ms produced similar results (data not shown) but we use the faster sampling so that our results might be applied to the higher frequency AMs

generated during initial prey detection in these fish (>10 Hz, Nelson and MacIver 1999). In addition, when given a step change in amplitude, the P-unit spike train is mostly adapted by 30 ms and, in its adapted state, responds linearly to the full range of intensities (Benda et al. 2005).

The corrected field gradient and the spike train response were therefore partitioned into 32 ms bins, overlapping by 16ms; a 3 ms delay was used between the start of the stimulus window and the start of the spike count window in order to account for latency/conduction delays (1.6 to 5.6ms: Bastian 1981b). The mean value of the stimulus in each bin was calculated and the mean EOD amplitude (without stimulation) subtracted from this value to give the mean stimulus change from the baseline EOD amplitude; we then computed the relative stimulus as the percent change of stimulus intensity from the baseline EOD amplitude and designate this as %ΔI. This was done to permit comparisons of P-unit responses across fish with differing EOD amplitudes. The mean spike count (unstimulated) or rate was also subtracted from the spike count per window to give the change in count (rate) from baseline; again we also computed the relative spike count or rate by dividing the change in spike count by the baseline count (rate). Thus we could compute either the absolute or relative change in the spike count of a P-unit in response to a relative change in stimulus intensity. These methods gave different results in some cases and which method is preferable depends on the putative decoding mechanism performed by downstream neurons (see below).

The spike counts were subsequently analysed in three ways: (a) The spike count mean and variance were computed across all repeated stimulus presentations for the same 32 ms window; in this case both the mean stimulus intensity and the stimulus slope are

constant for each bin, but the sample size is small – this is termed Vertical analysis (vertical divisions of Fig. 2a); (b) The spike count mean and variance were computed between amplitude increments of 1μV across the entire stimulus and the responses to the same mean intensities were grouped together. In this case the mean intensity within each window remains constant but its slope varies; the sample size is greatly increased. This method is termed Horizontal analysis and is based on the assumption that P-units code solely for intensity (Fig. 2a); (c) Lastly, we used the method (b) but separately analysed the spike counts occurring on up- and down- slopes of the signal; this is described as the Slope-Horizontal analysis (Fig. 2a).

The spike count (absolute or relative) was graphed versus the relative intensity change, where the middle 75% of all data points for the 5% contrast stimulus were used to calculate the slope of the line of best fit and the residuals computed. Any residual greater than 5x the standard deviation outside of the middle 75% data set were excluded in the determination of the coding range of the receptor. The standard deviations from the differing analyses were compared via ANOVA. The root mean square error (RMSE) was calculated using the line of best fit for all methods of analysis.

Data Analysis - High Frequency Stimulation

The covariance method, as outlined by Ruyter van Steveninck (de Ruyter van Steveninck and Bialek 1988) and used to characterize motion sensitive neurons in the fly (Brenner et al. 2000), retinal ganglion cells (Fairhall et al. 2006) and brainstem auditory neurons (Slee et al. 2005), was used for this analyses. We first computed the reverse correlation, or spike triggered average (STA), for the 20 ms (1 ms bins) preceding each

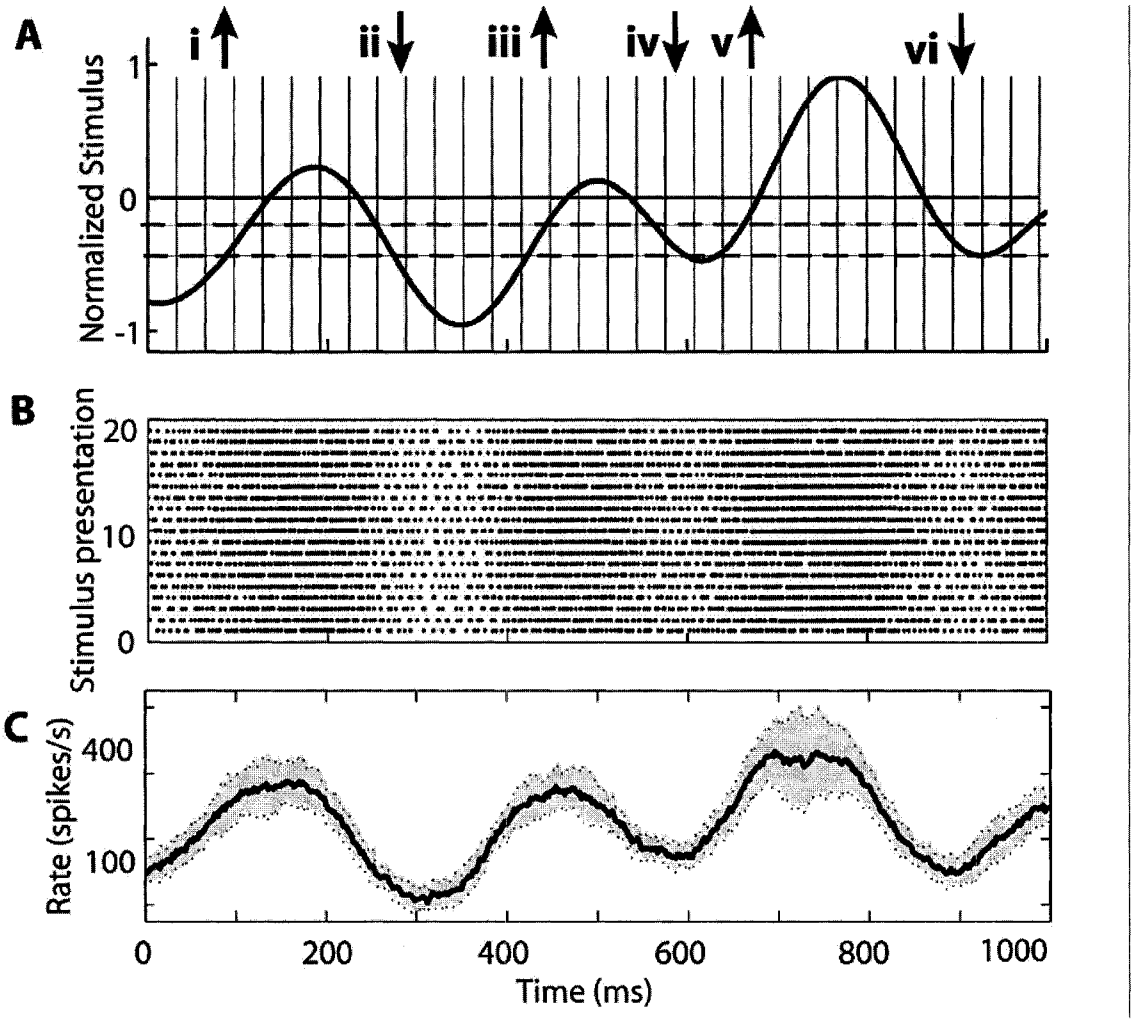

Figure 2: Overview of stimulation and analysis protocol. A. A one second sample of the global low frequency Gaussian noise stimulus (0-4 Hz RAM, 10% contrast). Vertical lines demonstrate the discretization into 32 ms time bins; the spike counts down each vertical bin served as the basis for the Vertical analysis. The dashed gray horizontal lines are one slice through the signal; the sections sampled have equal mean intensities but their slopes can vary considerably (e.g. compare ii with iv). Combining all samples (i-vi) served as the basis for the Horizontal analysis while separating positively (i, iii, v) and negatively (ii, iv, vi) slope regions served as the basis for Sloped-Horizontal analysis. B. Raster plot of a P-unit discharge in response to each stimulus presentation. Spikes are counted in 32 ms bins (Vertical) for each presentation. C. Mean time dependent firing rate estimated from the raster plot (32 ms bins) overlapped at 2 ms intervals. The firing rate faithfully follows this relatively strong stimulus (10% contrast); we note that these fish are capable of detecting contrasts of <1% (Nelson and MacIver, 1997). Gray band represents one standard deviation; the increased variability seen at the stimulus peak is due to the near saturation of the response for this unit.

spike; preliminary analysis showed that the STA declines to baseline by 20 ms and that longer time windows do not change the subsequent analysis (data not shown). In addition, an equal number of randomly sampled 20ms vectors were used to compute the mean stimulus independent of the occurrence of spikes. From these mean vectors we computed the covariance matrix of the STA (C_{spike} in the terminology of Brenner et al. 2000) and the covariance matrix of the random sampling of the stimulus (C_{prior} in the terminology of Brenner et al. 2000). Subtracting these matrices gives the covariance matrix associated with the stimulus induced spikes (ΔC in the terminology of Brenner et al. 2000).

We computed the eigenvalues and eigenvectors from the ΔC matrix. The relative contribution of each eigenvector was assessed by dividing the absolute value of the eigenvalue by the sum of absolute value of all the eigenvalues. Since the two largest eigenvalues (E1 and E2) accounted for 90-95% of the total variance, we confined further analysis to the associated eigenvectors; detailed analysis was carried out only for the eigenvector associated with the largest eigenvalue as discussed below.

We then computed the dot product of each 20 ms stimulus vector preceding a spike onto E1; this projection of the stimulus onto E1 estimates their similarity (S). This can be computed relative to the maximal EOD amplitude (this measure is used in the figures); it can also be computed as an absolute value (μV) since it is merely the E1 weighted mean of the signal. The same computation was carried out for the random sampling of 20 ms stimulus vectors. Both sets of projection values were then binned producing a probability density defined as the P(S | spike), for pre-spike stimulus

projection values, and P(S) for the random sampling, both of which are related to the relative intensity of the stimulus. Bayes theorem states:

$$\frac{P(spike|S)}{P(spike)} = \frac{P(S|spike)}{P(S)} \qquad \textit{Eqn 1}$$

where P(spike) is defined as the overall probability of spike discharge per EOD cycle (this is taken during stimulation and is nearly identical to the receptor's P-value) and P(spike|S) is proportional to a normalised rate as a function of the degree of similarity (S) to E1 (as described in Brenner et al. 2000; Slee et al. 2005); we also converted the conditional probability, P(spike|S), to a firing rate by multiplying it with the EOD frequency. P(S|spike) is readily calculated from the probability density of S (the projection of spike triggered stimuli onto E1). P(S) was calculated from the probability density of the randomly sampled stimuli. An f-I type relation was obtained by plotting the normalised firing rate versus S1 (Fig. 9B). We then carried out the calculations above for 20-second segments of the stimulus and computed the mean f-I curve; we then estimated the noise of this f-I curve by computing the standard deviation of individual f-I curves from the mean. Similar calculations were performed for the projection of the stimuli onto E2; the resulting f-I curves are generally linear with small slopes (data not shown) as expected from the small values of the E2 eigenvalue (see below). Since we are primarily interested in the response of P-units to stimulus intensity, these results are not further discussed.

Results

We recorded P-unit activity from a total of 54 fish. EOD frequency is highly correlated with the sex of the fish: males typically have EOD frequencies of 800-1000 Hz while females are between 600 and 800 Hz (Zakon et al. 2002). Since the EOD frequencies of the fish ranged from 630 to 970 Hz with approximately equal numbers above and below 800 Hz (data not shown), we assume that we were sampling from both sexes. No difference in P-unit properties were noted in this population as a function of EOD frequency.

We recorded a total of 310 units for baseline activity (36 fish), with a mean baseline spiking frequency of 199 ± 81Hz (range of 64 - 470 Hz); the fish's mean EOD frequency was 782 ± 90 Hz. The mean P value was 0.26 ± 0.11 (range of 0.06 to 0.60). Both the P value and baseline frequency distribution were well fit by a log-normal distribution with μ and σ values of -1.42 and 0.46 respectively (P values) and with μ and σ values 5.23 and 0.44 respectively (firing rate) (Fig. 1A, B); the modes of the distributions were 0.22 (P value) and 180Hz (the gamma distribution did not produce good fits, data not shown). The majority of P values were between 0.15 – 0.35 (76%).

It is clear that the P-value distribution is not Gaussian; although the excellent fit by a lognormal distribution might be coincidental, it is also possible that there is a deeper functional cause. A P-unit is composed of 25-40 receptor cells innervated by a single axon; each cell makes at least 16 synaptic contacts onto the P-unit axon (Bennett 1989). Firstly we assume that the number of synaptic sites of one receptor that release transmitter during one EOD cycle is a random variable drawn from some (unknown) probability distribution. We also assume that the electroreceptor cells are independent:

that is, the number of active synaptic sites at one receptor is uncorrelated with the number of active sites from another receptor for the same EOD cycle. The potential (postsynaptic) in the P unit afferent fiber at the time of a single EOD is also a random variable and it determines the P value of the unit. If the postsynaptic potential were proportional to the product of the number of active sites per receptor taken across all receptors, then the resulting P value distribution would be lognormal; if the postsynaptic potential were proportional to the sum of active sites, then a Gaussian distribution of P values would be expected. Detailed biophysical analysis of the tuberous electroreceptors will be required to test these speculative ideas.

Baseline Activity

Inter-spike interval distributions, as well as phase locking to the EOD were similar to previously reported results (Nelson et al. 1997; Ratnam and Nelson 2000; Xu et al. 1996). We recorded mainly non-bursty P units (71%, similar to:Xu et al. 1996) and, since analysis did not reveal any significant differences between bursting and non-bursting afferents, we pooled the results. The first order serial correlation coefficient (SCC) of the P units was negative with values similar to those previously reported (Ratnam and Nelson 2000); the value of the SCC was weakly negatively correlated to P value ($R^2 = -0.21$, $p < 0.03$).

As previously described (Ratnam and Nelson, 2000), P-unit Fano factor curves (variance/mean of the spike count as a function of counting time) decreased to a minimum (0.063 ± 0.053) occurring between 56-1000 ms (mean of 520 ± 277 ms) before increasing (Fig. 1C). Neither the counting window for the Fano factor minimum nor its

value were related to the afferent's P value (not significant, $p > 0.10$). At short intervals (<50ms), P value was strongly inversely related to the Fano factor, and significant negative correlations persisted to 250 ms (Fig. 1D).

P unit response to low frequency noise (fc = 4Hz)

Low frequency signals were presented to 77 P-units (11 fish). The mean spike count per 32 ms appears to faithfully track the stimulus intensity of the 0-4Hz RAM stimulus (comparing Fig. 2A to 2C). Plotting either absolute or relative mean change in spike count versus relative intensity revealed a central linear range, representing the effective coding range of the receptor, bounded by sections of zero-slope and/or irregular spiking indicative of saturation due to very low or high intensities (Fig. 3A).

Linear fits were initially performed to the central region (using 75% of the data surrounding the baseline spike count) and then extrapolated outwards. Very good linear fits were achieved for all P units ($R^2 = 0.94 \pm 0.14$, $p < 0.005$). The residuals (Fig. 3B) calculated from the linear fit were then used to define the lower and upper limits for linear coding for each P unit: residuals outside of the central region and larger than 4x the central residual standard deviation (SD) were excluded. The linear coding range of these neurons is independent of P value and stimulus contrast (the minimum and maximum intensities are -17% ± 7.5% and 17% ± 8.8% respectively) of the baseline EOD amplitude; spiking is silenced at the low intensities and saturated at approximately double the baseline firing rate. The SD did not change significantly over the entire coding range (Fig. 3A, 6A). This coding range is sufficient to encompass the full intensity range of low

frequency signals expected during electrolocation (Babineau et al. 2006; Chen et al. 2005).

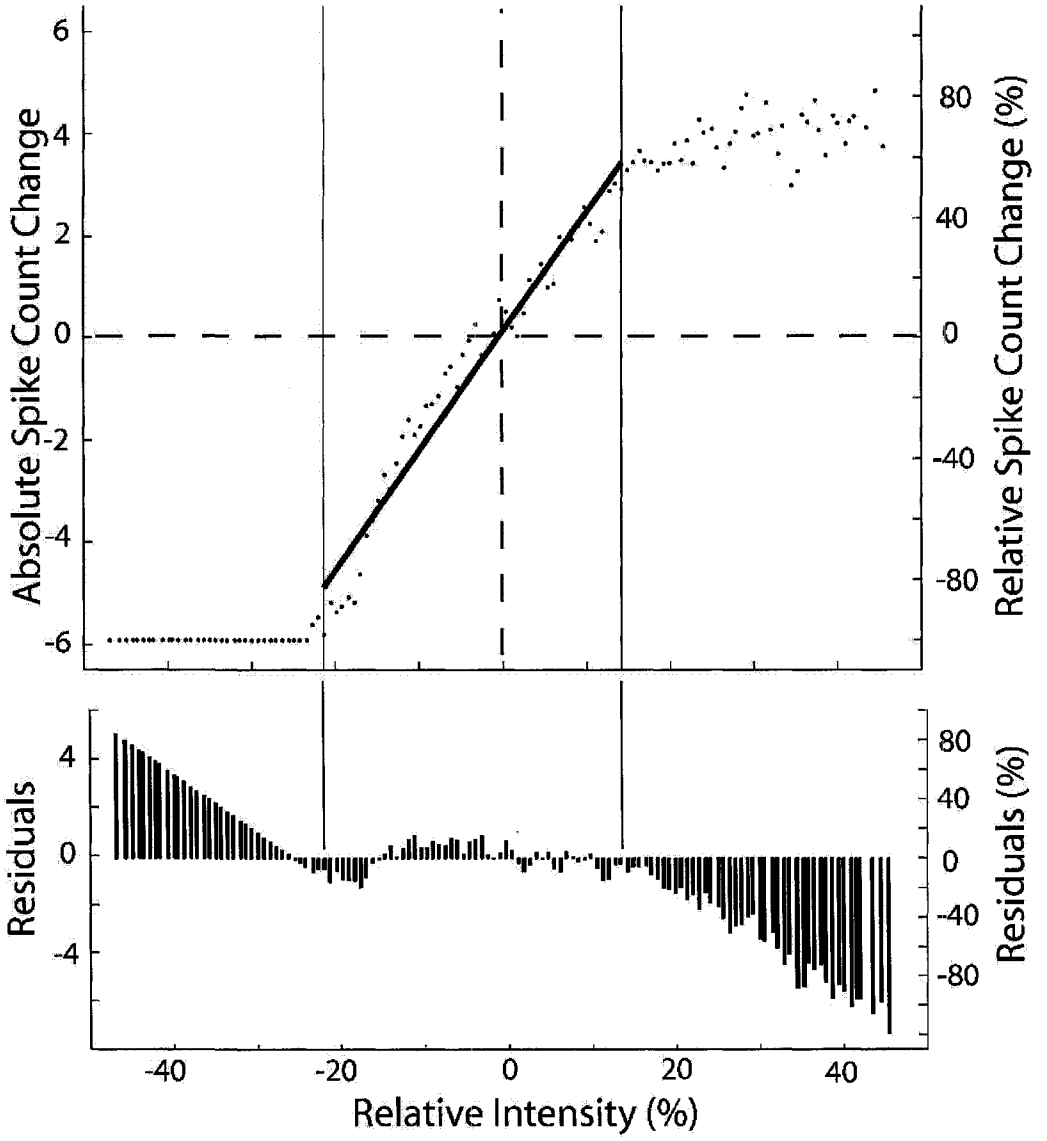

Figure 3: A. F-I plot. The mean change in spike count within 32 ms is plotted against the relative change of stimulus intensity (10% contrast); a linear fit to the central region (thick solid line) was used to compute P-unit gain (slope) and range. The coding range of this unit is indicated by the thin vertical lines. B. Residuals of the fit when extended over the entire stimulus range.

Gain is positively related with P value when absolute spike counts are used (range: 0.035 - 0.447 spikes/32ms /%ΔI, avg. gain = 0.197 spikes/32ms /%ΔI, $R^2 = 0.55$ where $p < 0.01$). Following the convention in this field we convert the rate to spikes/sec ((Fig. 4A) range: 1.1 – 14.0 spikes/sec /%ΔI, avg. gain = 6.16 spikes/sec /%ΔI)). This suggests that if target pyramidal cells in the electrosensory lateral line lobe (ELL) can detect absolute changes (± 1 spike/sec) in the P-unit spike count, then high P value receptors will be most sensitive to small changes in intensity. As noted in the methods section, percent changes in intensity were used to compare between fish with varying EOD amplitudes. We repeated these calculations for absolute (μV) changes in intensity: for a 1 μV/cm change (averaged over 32 ms), we expect (averaged across all P values) an extra 0.32 ± 0.17 spikes/sec. This value is lower than the ~1 extra spike/sec/μV/cm given in earlier reports (Bastian 1981a; Nelson et al. 1997). It is possible that by extrapolating the gain-frequency relationship down from minimum experimental intensities of 63μV/cm (Bastian 1981a) and 10μV/cm (Nelson et al. 1997), gain at 1μV/cm is overestimated. The discrepancy might also, in part, be due to differences in methodology: Bastian used sinusoidal AMs (as opposed to RAMs) with large increases in intensity and extrapolated down to microvolt levels. Nelson based his estimates on the use of sinusoidal amplitude modulations and P-unit models that were in turn calibrated by Bastian's earlier data. This disparity strongly affects the number of downstream neurons required to detect small changes in input; we further discuss this discrepancy after describing the results of our covariance analysis below (also see Discussion).

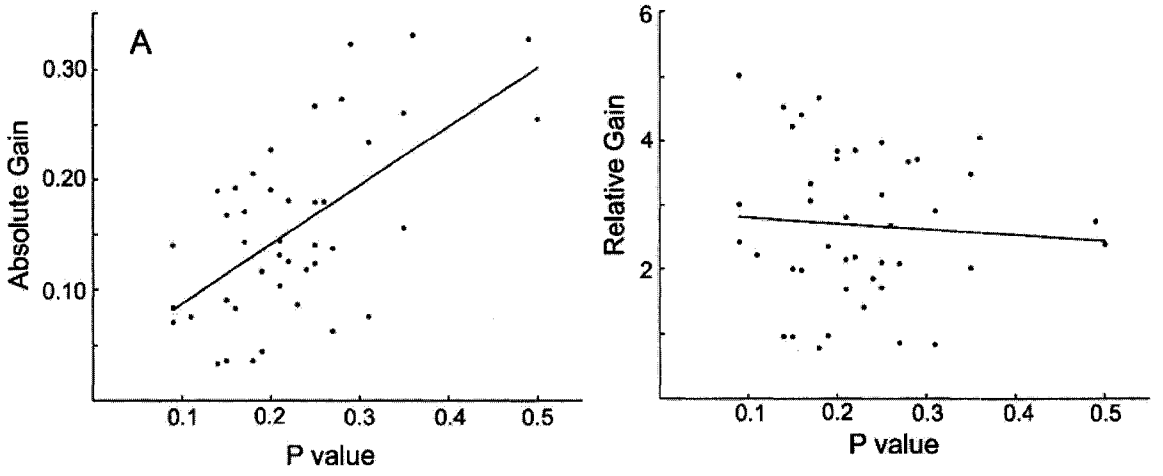

Figure 4: Gain versus P value. A. When absolute spike count within 32ms are used, the gain of a P-unit is positively correlated with its P value: $R^2 = 0.59$ at 5% contrast stimulation ($p < 0.001$), $R^2 = 0.67$ at 10% contrast stimulation ($p < 0.001$). B. For relative spike counts the gain is independent of P value.

The relative spike count per relative intensity (i.e. relative gain) has no relationship to the baseline spiking frequency or P value (range: 0.76 - 8.01 %spikes/%ΔI (Fig. 4B)). A relative measure would be appropriate if downstream neurons normalised the P-unit baseline input by, for example, synaptic depression (Abbott et al. 1997). Since this possibility is entirely speculative, we follow previous authors (Bastian 1981a; Nelson et al. 1997) and present results solely as absolute spike count and spike rate.

P-units show strong adaptation to sustained or slowly changing input (Benda et al. 2005; Nelson et al. 1997; Xu et al. 1996) implying that the extent of adaptation might be different on the positive and negative slope of the stimulus waveform and contribute to the variability of the P-unit response. We therefore computed the f-I curves independently for the positive and negative slopes of the stimulus (sloped-horizontal analysis, Fig. 5). The coding range and the defined maximum and minimum firing frequencies were the same regardless of the sign of the stimulus slope and were not

significantly different from those values computed for the entire stimulus and across various stimulus contrasts.

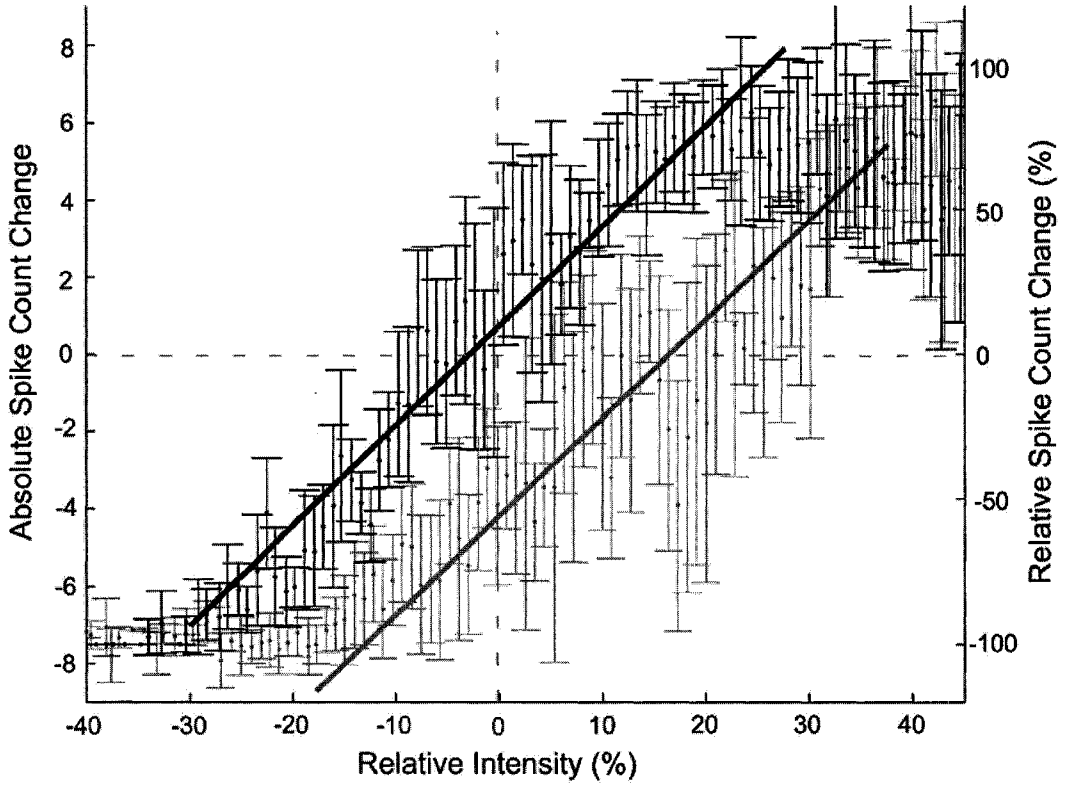

Figure 5: F-I curves for positive (black line) and negative (gray line) stimulus slopes with error bars (standard deviation) and best fit lines (black and grey solid lines respectively). The f-I gain is the same for both slopes but there is an offset by a spike count bias; the f-I curve for the entire data set shown in Fig. 3 would lie precisely in the middle of these curves. The intensity range (ends of best fit lines) are equal and independent of baseline P value.

The gain of the f-I curves was the same for horizontal and sloped-horizontal curve analyses. However, the curve generated from the positive slope sections of the stimulus was leftward displaced in comparison with the curve from the negative slope sections while the negative slope sections were rightward displaced (8.5 ± 4.5 percent intensity difference; black bar, Fig 5); the linear fit for the horizontal analysis was located symmetrically between these curves (data not shown). This result is consistent with the

dynamics of P-unit adaptation since the firing rate is low at the onset of the positive slope, reducing adaptation and therefore causing a shift of the neuron's f-I curve to lower intensities (Benda and Herz 2003). This result implies that a linear rate code estimate of signal intensity will be biased if the gain for the horizontal analysis is solely used in its computation (Fig. 3A).

As observed for the curves generated from the horizontal analysis, the standard deviation (noise) for the sloped-horizontal curves remained constant over the entire linear coding range. However, the noise for the horizontal curve is greater, over the entire linear coding range, than that of the sloped-horizontal f-I curve (Fig. 6A, C). Under the assumption that the standard deviation reflects P-unit noise, this implies that noise levels will be reduced if a central decoder could separate P-unit spikes emitted during the positive versus negative slopes of the stimulus. This idea was further investigated by computing the spike count variability around the mean of the baseline discharge in response to varying levels of contrast. This spike count distribution (for all conditions) can be well approximated as Gaussian (Fig. 6B) and we have previously noted that the spontaneous variability might represent noise since it occurs independent of stimulation (Chacron et al. 2001). The standard deviation of the spike count computed vertically (no variation in stimulus slope) was not significantly different from that of baseline variability (0.71 ± 0.18 spikes/32ms [22.16 ± 5.5 spikes/sec] versus 0.68 ± 0.18 spikes/32ms [21.33 ± 5.5 spikes/sec], Fig. 6C).

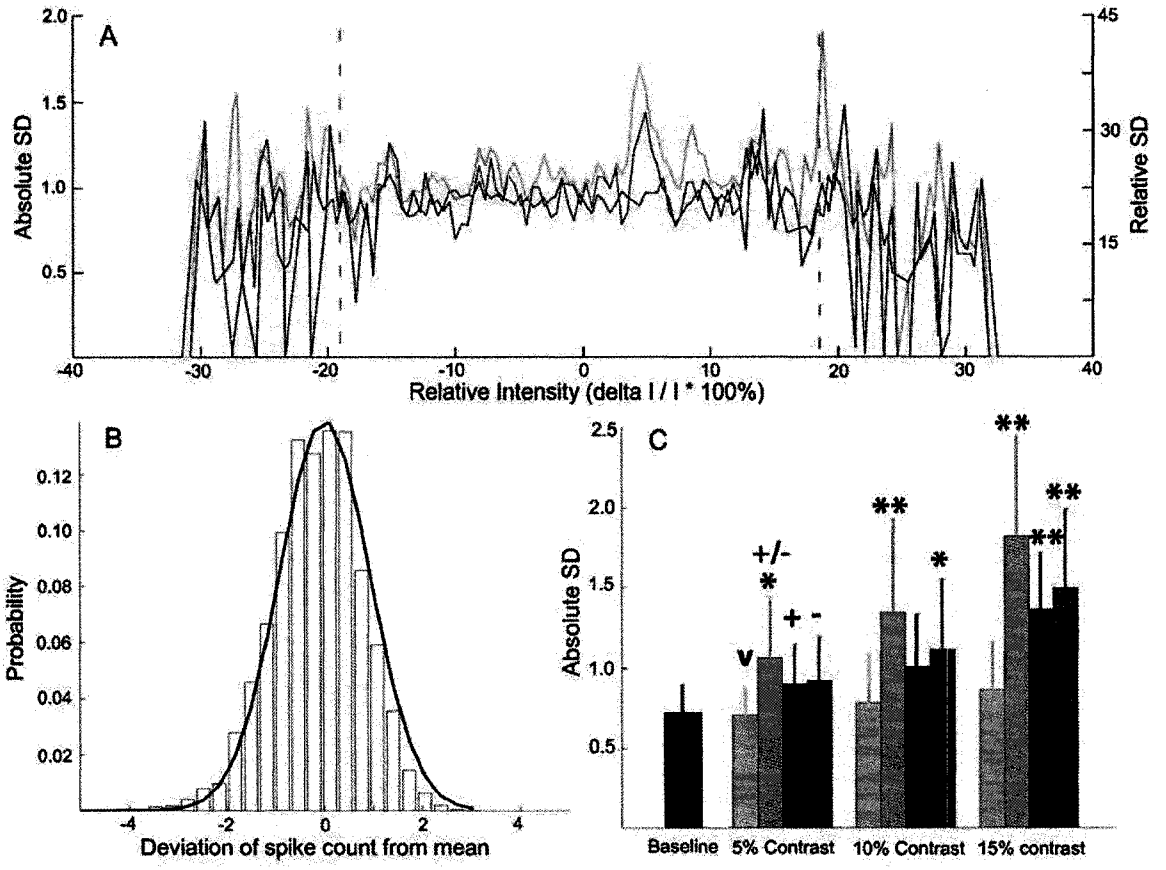

Figure 6: A. Standard deviation of the spike count (within 32ms) over the coding range for counts pooled over the entire stimulus (green) versus separate counts for the positive (blue) and negative (red) slopes of the stimulus. The standard deviation becomes more variable outside the coding range (dashed gray vertical lines) because of either erratic discharge or saturation effects. Note that the standard deviation of the spike counts for both the positive and negative slopes are typically lower than those for the entire stimulus. B. Spike count distribution of stimulated discharge for 32 ms (mean subtracted) of a typical P-unit averaged across all bins (Vertical analysis, 5% contrast). Black line is the Gaussian fit to this data. C. Standard deviation of the absolute spike count within 32ms for baseline discharge (black), Vertical (v, light blue), Horizontal (+/-, green), positive stimulus slope (+, blue) and negative stimulus slope (-, red) for contrasts ranging from 5-15%. Significance is based on comparisons with the vertical standard deviation within a given contrast, with one-star ≡ $p<0.05$ and two-stars ≡ $p<0.01$ (ANOVA). The vertical standard deviation is not significantly different from that of the spontaneous discharge at all contrasts. The results are similar for the relative spike count.

In contrast, the horizontally computed variance was significantly higher and increased with the contrast (as previously reported by Wessel et al. 1996): at 5% contrast, horizontal noise (0.91 ± 0.33 spikes/32ms [28.40 ± 10.4 spikes/sec], $p < 0.001$) is 40%

greater than the vertical noise, and increases by 40% for each 5% increase in contrast. Furthermore, the noise for the total stimulus was, at any contrast, greater than that computed for positive and negative slope: the sloped-horizontal noise (0.74 ± 0.21 spikes/32ms [23.03 ± 6.5 spikes/sec]) is only 18% greater than the vertical noise and increases 18% for each 5% increase in contrast. Similar results were obtained when absolute or relative spike counts were used (data not shown).

Since an increase in contrast will increase the variability in stimulus slope, this data suggests that at least a portion of the "noise" may be due to the P-unit responding to variations in stimulus slope. By separating the stimulus into increasing and decreasing changes in amplitude, the variability is reduced compared to horizontally computed noise. In fact, in the limit of the very low contrasts that occur during prey detection (<2%, Nelson and MacIver 1999), additive Gaussian noise is equal to the variance of the baseline spike count (even at 5% contrast, vertical noise: 0.71 ± 0.18 spikes/32ms [22.16 ± 5.5 spikes/sec] and sloped noise: 0.74 ± 0.21 spikes/32ms [23.03 ± 6.5 spikes/sec] were not significantly different from baseline variability (0.68 ± 0.18 spikes/32ms [21.33 ± 5.5 spikes/sec]); variability of baseline discharge is therefore a valid approximation of the noise in rate coding models of the P-unit response to weak low frequency signals.

The effect of eliminating the bias and reducing the variance can be assessed from the accuracy of stimulus reconstructions based on the computed linear f-I curves. When reconstructing the stimulus using the 5% contrast gain (to avoid the saturating regions), the mean square error between the original stimulus and its reconstruction is reduced >3-fold when positive/negative slope are taken into account (absolute spike count: total

RMSE = 9.37 ± 4.74μV; sloped RMSE = 2.86 ± 0.80μV); similar results were obtained when using the relative spike count (data not shown).

Fc = 50 Hz Stimulus-Response Characteristics

The 0-50 Hz signals were presented to 45 P-units (7 fish). Our analysis suggested that the P-units were responding to both the intensity and slope of the low frequency RAM signals; we therefore turned to a recently developed method that can explicitly decompose the spiking response of a neuron to a linear combination of time-dependent vectors. We used the covariance method of de Ruyter van Steveninck et al (1988) and Brenner et al. (2000) with high frequency RAMs (50 Hz cut-off) as stimuli. We first computed the spike triggered average (STA); this vector is positive just preceding a spike and rapidly drops to negative value before settling to 0 (baseline EOD amplitude) by 20 ms (Fig. 7A), as previously reported in earlier studies of a related electric fish (Wessel et al. 1996). The shape of the STA and its spectrum are independent of EOD frequency and P value (data not shown). We also used the STA (corrected for the autocorrelation/power spectrum of the spike train, Gabbiani 1996; Wessel et al. 1996) to evaluate the error of linear signal reconstruction; we found coding fraction values (range Cf = 0.640 – 0.925, mean Cf = 0.798 ± 0.089) consistent with earlier studies on a related electric fish (Wessel et al. 1996).

The eigenvector (E1), corresponding to the largest eigenvalue of the spike triggered covariance matrix, was very similar to the STA (Fig. 7A). The STA, and therefore E1, represents the time-weighted intensity - positive for ~6 ms preceding a spike and negative back to ~20 ms - of the stimulus that is likely to evoke P-unit spiking

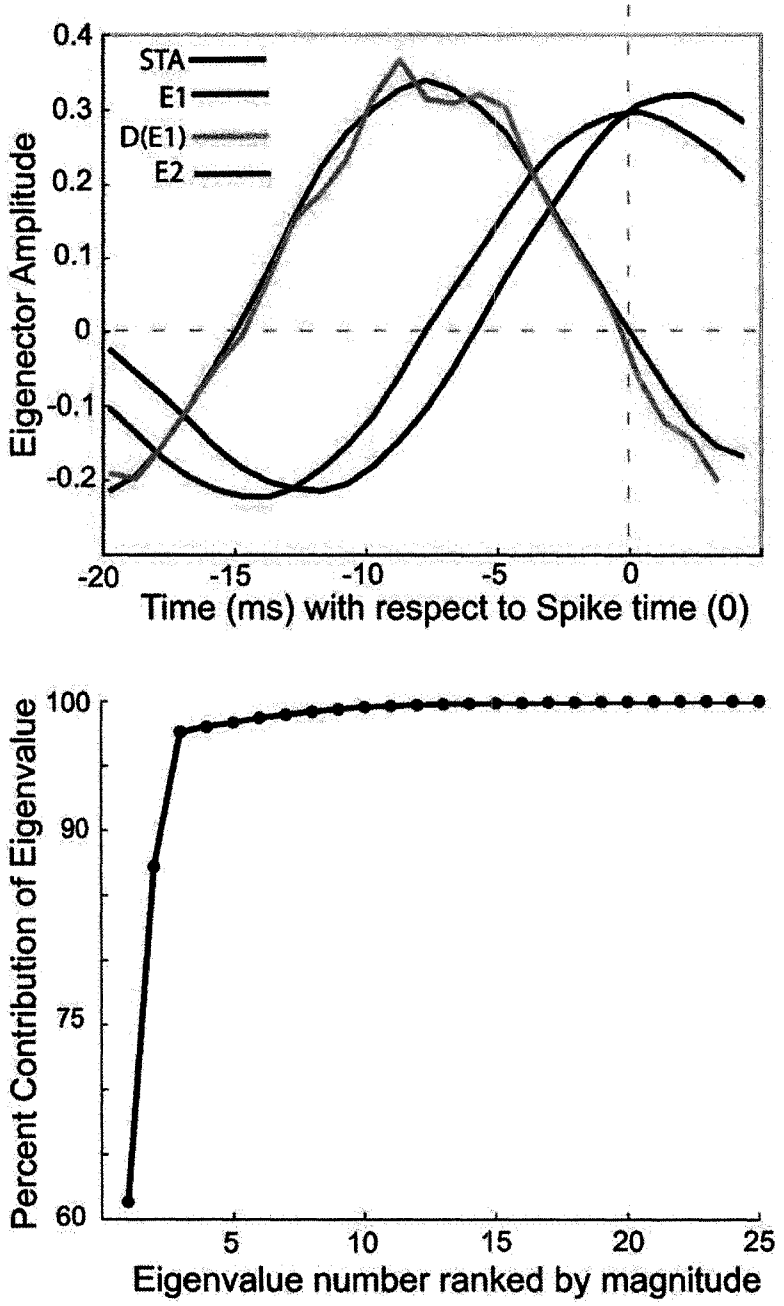

Figure 7: Top: The spike-triggered average (STA, black) is nearly identical to the first eigenvector (E1, blue); the second eigenvector (E2, green) resembles the derivative of the E1 (red). The STA decays to 0 by 20 ms and no change in E1 or E2 was seen when STA was calculated for longer prespike intervals. Bottom: Cumulative percent strength of the eigenvalues. The first and second eigenvalues account for ~87% of the variance in the response for this P-unit.

and accounts for most of the variance of the response (65-85%) for all P values. The second eigenvector (E2), corresponding to the second highest eigenvalue, resembles the derivative of the STA and is therefore a measure of the local slope or change of the stimulus (Fig. 7A).

The relative contribution of the covariance matrix eigenvalues to the total variance drops rapidly and, as reported in other sensory systems (Brenner et al. 2000; Slee et al. 2005), the first two eigenvalues account for, on average, 92% percent of the total variance (85 – 95%) (Fig. 7B). Similar results were obtained when 0-100 Hz RAMs were used (data not shown).

The relative contribution of the first and second eigenvalue varied systematically with P value so that higher P value receptors tend to have a stronger E1 contribution while those with low P values have a larger contribution from the second eigenvector (though still less than E1, and E2 drops to almost zero at higher P values) ($R^2 = 0.52$, $p < 0.02$, Fig. 8). This suggests that low P value receptors are better suited to signal changes of intensity, whereas high P value receptors can code almost entirely for the first eigenvector (intensity). Since E1 is closest to the "intensity" variable of F-I curves, our subsequent analysis is focused on the E1 vector. The contribution of E1 to the variance (mean = 76%) is similar to the stimulus-response coherence of P-units (60-80% for frequencies up to 50 Hz; Chacron et al. 2005). These are linear methods and both rely on the cross-correlation of stimulus and evoked spike train. Although subsequent data analysis is different (covariance matrix decomposition versus Fourier transform to the frequency domain) it is reassuring that they nonetheless give comparable results.

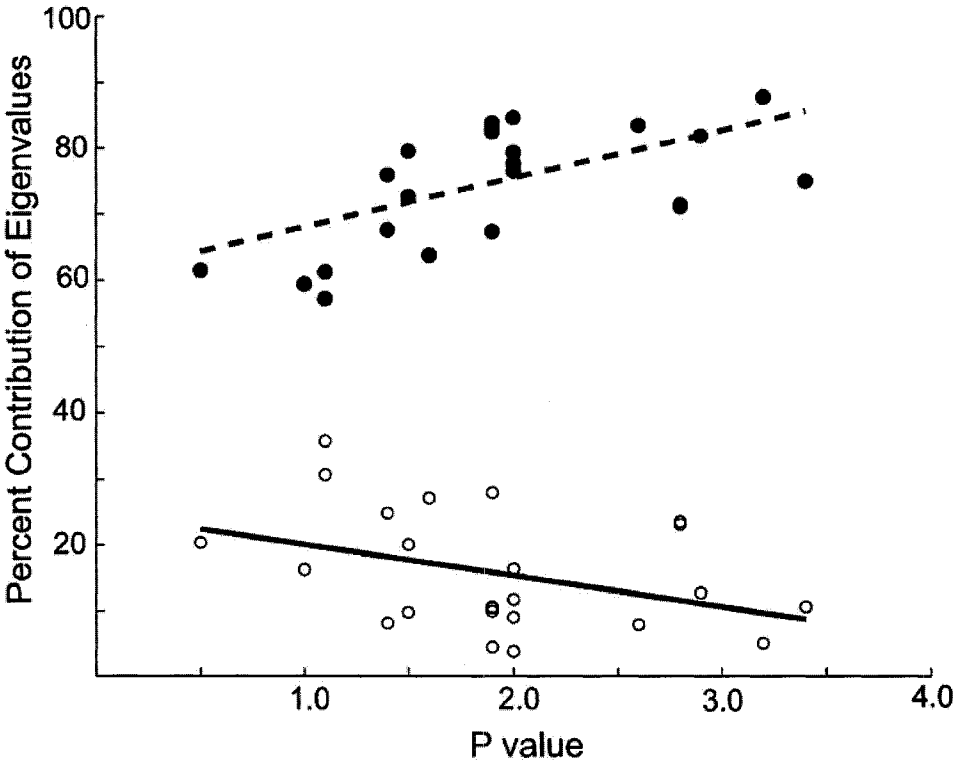

Figure 8: Relative contribution of the E1 and E2 eigenvalues to total variance as a function of P-value. E1 increases with P-value while E2 decreases. The sum of E1 and E2 is constant at 90-95% across all P-values (not shown).

Projecting the pre-spike vectors onto E1 computes its similarity to E1 and thus to the time-weighted intensity; we designate this value as the normalised relative intensity (S). Estimating the probability of a spike given the occurrence of E1 provides a measure of the spike rate. These quantities are connected via Bayes theorem and, as previously described (Brenner et al. 2000), were used to compute a normalised f-I curve by plotting the normalised firing rate versus the normalised relative intensity (see Methods). In order to estimate the noise remaining in this derived f-I curve, we computed the f-I relation for 20-second segments of the recordings and calculated the standard deviation of the curve from the variations of individual curves with respect to the mean curve.

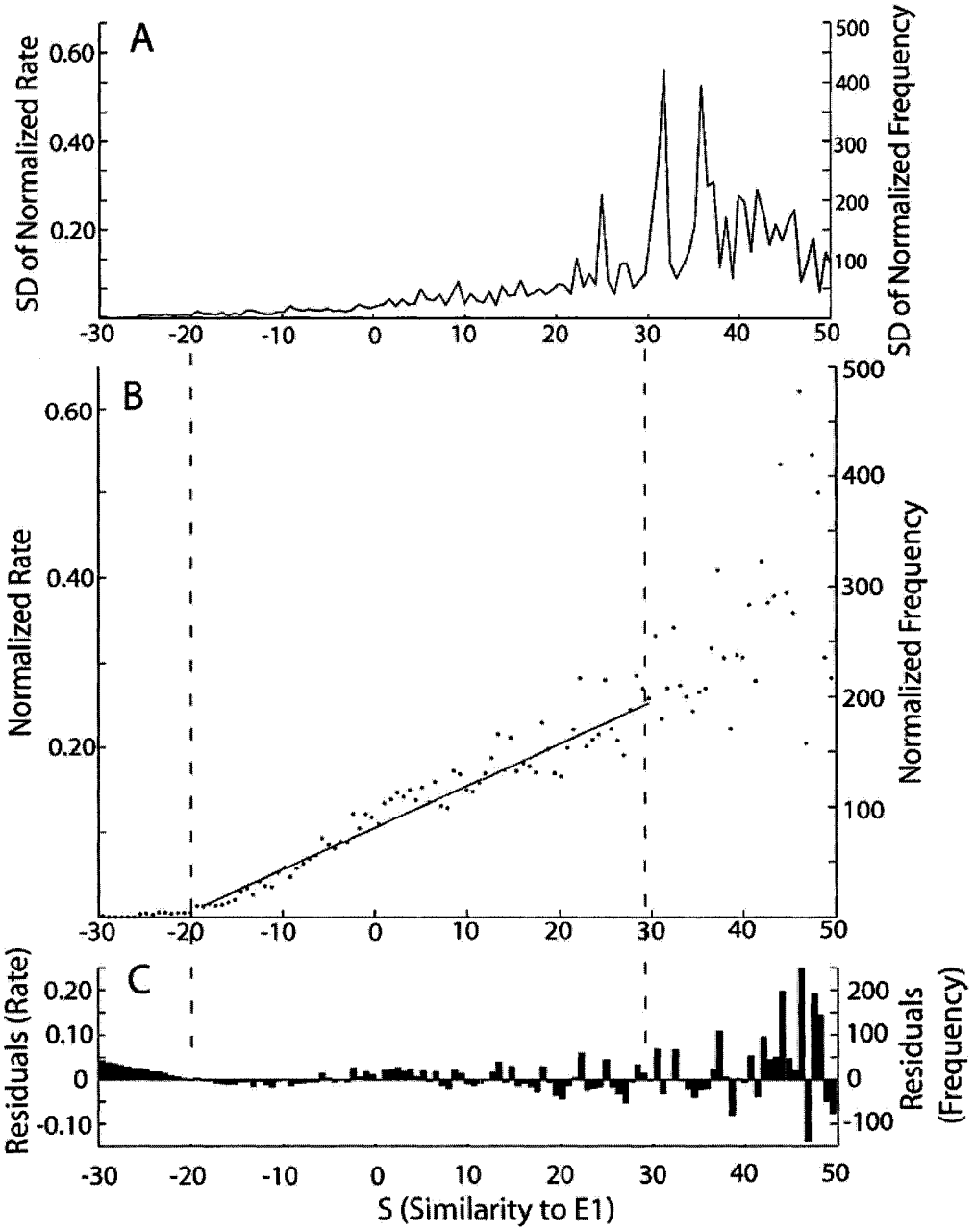

Figure 9: A. Standard deviation of normalized f-I plot, derived by creating 9 equal sized time segments, calculating the normalized rate within each, and the standard deviation between them. B. Normalized f-I curve showing the relation between normalized firing rate to the similarity of the stimulus to E1.The solid line is the linear fit within the coding range, defined as the region between saturation and when the standard deviation is larger than the firing rate. C. Residuals from the linear fit.

Plotting S1 versus the normalised relative intensity generates a linear relationship (Fig. 9). This linear region is bounded by regions of saturation or highly variable spiking similar to the results for the $f_c = 4$ Hz stimulus, defined by the largest region where the mean normalised spike count exceeds the noise. The normalised relative intensity coding range has average minimum and maximum values of $-17.99 \pm 10.7\%$ and $18.85 \pm 10.6\%$ similar to those for 4 Hz stimulus. As previously described for f-I curves derived from 4 Hz stimuli, the P unit is silenced at the lowest S values (when the signal is most dissimilar to E1) and is approximately double the baseline firing rate at the upper end of the coding range. The maximum normalised rate therefore increases with baseline frequency ($R^2 = 0.65$, $p < 0.005$). Neither the normalised relative intensity (S) range, nor the normalised gain (range: 2.84 – 13.02 spikes/sec / %ΔI, avg. 5.76 ± 3.04 spikes/sec / %ΔI) were related to the P-unit baseline frequency. Further, both intensity range and normalised gain are similar to the 4 Hz gain data suggesting that the Brenner et al method produces f-I curves comparable to those calculated with low frequency RAMs and the counting window method.

We therefore attempted to calculate the absolute gain of this f-I curve: the increase in spike count to a 1 μV/cm increase in stimulus intensity from the S projection values. A 1 μV change in intensity causes a 2.38 ± 1.09 spikes/sec/μV change in firing rate, or a 7.3-fold increase over the 4 Hz gain. Earlier studies have also shown that gain increases with frequency (Bastian 1981a) but estimate a slightly lower (~5-6 fold) increase in going from 4 to 50 Hz (Chacron et al. 2005a; Nelson et al. 1997).

Benda et al. (2005) computed the f-I curves at both the onset of step changes in EOD amplitude (f_0) and after adaptation (f_∞). Both f_0 and f_∞ are linear with slopes of 0.32

spikes/sec/μV (this paper: 0.32 spikes/sec/μV) and 1.97 Hz/μV (this paper: 2.38 spikes/sec/μV) respectively (these were computed from the data published in Benda et al. 2005) giving a six-fold increase. Our low frequency (4 Hz) signals are similar to the f_∞ condition with respect to the state of adaptation of the P-units; similarly, our 50 Hz stimuli are similar to the f_0 condition. It is therefore not surprising that the Benda et al. estimates are also very similar to those calculated for our low and high frequency stimuli, although again we have estimated slightly higher gain for the 50 Hz RAMs. Our low estimates for mean low frequency gain might therefore be more accurate than previously reported values. However all estimates of the relative frequency dependence of gain are in approximate agreement. Both the method employed in this paper and that of Benda et al. (2005) showed a large variability in the gain of individual P-units. It is therefore also possible that the P-unit population can fractionate the large intensity range of electrosensory signals; while this might, in principle, improve coding for both strong and weak signals, it would also mean that a decoder might not be able to utilize simple averaging over the entire population. We do not therefore consider this more complicated possibility below.

The standard deviation of the normalised firing rate increases with the value of S ($R^2 = 0.49$, $p < 0.001$), ranging from 15-65% of the normalised firing rate. This is likely due to undersampling - there are few samples for high values of S which makes the values of P(S) very small and variable; since P(S) is used in the denominator (Eqn. #1) this variability becomes magnified. For small natural electrolocation signals (within 2% of baseline EOD amplitude, Nelson and MacIver 1999) appropriate to the detection of prey items, the SD is 22.37 ± 4.04 spikes/sec. This value is nearly identical to the SD of

the baseline spike count (over 32 ms) suggesting that noise due to baseline variability of P-unit discharge is the final limit for rate coding in the electrosensory system.

Discussion

The coding of time varying signals by P-unit electroreceptors of high frequency wave type electric fish has been the subject of numerous investigations (Bastian 1981a; Benda et al. 2005; Benda et al. 2006; Chacron et al. 2001; Chacron et al. 2005a; Kreiman et al. 2000; Ludtke and Nelson 2006; Nelson et al. 1997; Ratnam and Nelson 2000; Wessel et al. 1996; Xu et al. 1996). Although different types of analysis have been used, the overall conclusion is that P-units are good linear encoders over a wide frequency range and that their gain increases with frequency. In *Eigenmannia*, calculation of the optimal spike triggered average was used to compute the percentage of the signal variance captured by the P-unit discharge (coding fraction) and coding fractions up to 0.80 have been reported (Wessel et al. 1996). In *A. leptorhynchus* coherence has been used to demonstrate that linear encoding by P units can capture about 70% of the signal variability over a wide frequency range (Chacron et al. 2005); further, Chacron (Chacron 2006) compared stimulus-response to response-response coherence to conclude that little additional information could be extracted by a nonlinear filter.

We have used a more traditional approach, the construction of f-I curves, to confirm that P-units are linear encoders; further, the variance of the spike count response was independent of the stimulus intensity, suggesting that an additive noise model is suitable. The advantage of this approach is that it can be immediately linked to a simple putative decoding mechanism: pyramidal cell targets can integrate the numerous P-unit inputs over a time window appropriate to the maximal signal frequency. For the sensory input expected during the fish's prey capture behavior (Nelson and MacIver 1999), integration times of 25-200 ms would be appropriate. Since the response of P-units is

statistically independent for both baseline and low frequency input (Benda et al. 2006; Chacron et al. 2005a), the input noise will scale as the square root of the number of P units converging onto a pyramidal cell (see below).

F-I curves are often constructed using constant inputs; we have used the Brenner et al. (2000) method for slowly varying input appropriate to the frequencies expected in the final phases of prey capture (4 Hz cut-off frequency). We find that the variance and bias of the response are highly dependent on variations in the slope of the signal. This is not surprising since the P-unit's high pass filter response with a cut-off frequency at 1 Hz as described by Nelson et al. (1997) makes them sensitive to the slope of the stimulus in addition to the stimulus intensity. A lower bound on the variance of the P-unit spike count is set by the variance of the baseline discharge (Chacron et al. 2001) and depends on the length of the counting window (Fig. 1 and Nelson et al. 1997). For weak perturbations (<5% contrast as expected for prey, Nelson and MacIver 1999) the spike count variance approaches this lower bound only if computed separately for responses to the positive and negative slopes of the signal. Separating the response to positive and negative slopes also eliminates a small bias in the response and, together with the reduced variability, leads to far better stimulus estimation. Although separating the stimulus into regions of positive and negative slope is a nonlinear operation, it is performed automatically by the circuitry of the ELL; ELL pyramidal cells can be divided into two major classes- basilar and non-basilar pyramidal cells (Maler 1979; Maler et al. 1981; Saunders and Bastian 1984). Basilar pyramidal cells (E cells) respond on the stimulus upstroke while non-basilar pyramidal cells (I cells) respond on the downstroke (Heiligenberg and Partridge 1981).

Weak Signal Detection

Behavioral experiments have demonstrated that *A. leptorhynchus* can detect signals <1 μV and perhaps as low as 0.2 μV (Bastian 1981a; Knudsen 1974; Nelson and MacIver 1999); in order to assess how well a simple linear rate coding P-unit model performed, we assessed its ability to discriminate 1 μV changes in stimulus intensity. We used the discriminant ($d' = |R_1-R_2|/SD$), where R_1 and R_2 are the spike count (SC) at 0 μV and 1 μV respectively and SD the standard deviation of the spike count (Dayan and Abbott 2001) as a ratio measure of neuronal sensitivity to inherent noise. Using the mean 4Hz Horizontal gain, 1 μV produces a mean change of 0.32 ± 0.17 spikes / second, and the mean sloped horizontal SD is 23.03 ± 6.5 spikes / second. By calculating the ΔSC / SD ratio for each neuron individually, the average ratio is 0.0108 ± 0.0213. Since P units are independent (Chacron et al. 2001; Benda et al. 2006), the SD will decrease with the square root of the number of neurons; therefore a fish needs ~10,700 P units to accurately detect 1 μV, a number greater than the number of tuberous receptors on one side of the body (7000-8000, Carr et al. 1982).

These fish can take up to 200 ms to scan past a prey item and previous research has assumed that this is the integration time for detection (Ratnam and Nelson 2000). Because our stimulus was a 4 Hz RAM we cannot directly estimate d' for such long stimuli. We assume, for the weak perturbations used, that both the spike count and its standard deviation would scale with the counting time window in the same way as for baseline activity (as per the Fano factor plot in Fig. 1). In this case the spike count would increase six fold while the SD would double when the window went from 32 to 200 ms. This would result in a three fold increase in d' and, consequently a nine fold decrease in

the number of neurons to ~1190. This level of convergence does in fact occur in the lateral segment of the ELL (Maler, *unpub. obs.*). However, while the simple f-I curve might explain the detection of a 1μV change, it cannot explain detection levels of ~0.2 μV.

The statistical structure of the P unit spike train is highly constrained by adaptation that decays over many EOD cycles (Ratnam and Nelson 2000; Chacron et al. 2001). Recent studies (Goense and Ratnam 2003; Kreiman et al. 2000) have demonstrated that single extra spikes inserted into a P-unit spike train might be readily detected with few false alarms. If the decoder used by these authors could be scaled up to a large population of P units, then the system sensitivity might be sufficient to detect <1 μV signals; it is not clear whether simple averaging would work however since it would require the "extra" spikes be added to all P units at roughly the same time and it is therefore not clear how such a population decoder would operate. An additional source of information for detecting prey items might be ampullary input but even this might not be sufficient (MacIver et al. 2001). A recent paper (Ludtke and Nelson 2006) has suggested that an optimal estimator operating over the electroreceptor population could use Punit inter-spike interval correlations to greatly improve detection of weak signals; this information is eliminated when rate coding f-I curves are used. The requirement for this method to work was the estimation of conditional probabilities by the dynamics of short term plasticity of P-unit synapses; there is, as yet, no experimental verification of this interesting possibility.

Our results from the covariance analysis of the P-unit response to high-frequency stimuli (cut-off frequency 50 Hz) suggest another potential mechanism by which the

electrosensory system might detect such weak signals. If the electrosensory decoder could extract the first eigenvector from a P-unit spike train response, then it would encode a 1 μV increase with, on average, an extra ~2-3 spikes/sec with a SD of ~22spikes/sec. This reduces the number of P units needed to detect 1 μV fluctuations around baseline EOD amplitude to only ~200 neurons (calculated for each unit and then averaged across units). In this case even the detection of 0.2 μV would be possible for the lateral segment of the ELL since convergence ratios of 1000 are seen in this map (Maler, *unpub. obs.*).

Note, that the high frequency stimuli necessary for the covariance method probe the P-unit input-output relation in a different frequency band than the low frequency stimuli used for constructing f-I curves. As a consequence, these two complementary methods reveal signal transmission properties due to different mechanisms. Nelson et al. 1997 characterised the gain of the P-unit's transfer function with two high-pass filters. The first filter had a cut-off frequency at about 25 Hz. This filter is due to rapid spike frequency adaptation as described in Benda et al. 2005 and this filter gives rise to the E1 and E2 components obtained from the covariance analysis of the spike response to high frequency stimuli. The second filter had a cut-off frequency of about 1 Hz, and it is this filter that causes the f-I curve computed from the response to the low-frequency stimuli to vary with the slope of the stimulus.

The covariance analysis we performed on low level electroreceptor responses is similar to previous studies of low level filtering by visual (Brenner et al. 2000) and auditory (Slee et al. 2005) neurons and reaches remarkably similar conclusions; a recent study has also reported similar results for a subset of retinal ganglion cells (Fairhall et al.

2006). First, there are two dominant filters (eigenvectors): E1 is a smoothing filter (for velocity or intensity) operating over a short time range and resembling the spike triggered average; E2 is approximately the time derivative of the first eigenvector and therefore responds to rapid changes of the stimulus. Second, parsing the input with these filters reduces the response variability and/or increases the information transmitted. This is intuitively clear since, as already noted by Brenner et al., much of the "noise" in standard f-I curves comes from the fact that many sensory neurons respond to both the intensity (velocity in their case) of a signal and the change of intensity (acceleration in their case). These stimulus attributes are confounded in classic f-I curves. Therefore low level sensory processing would be far more efficient if downstream decoders could do an eigenvector decomposition of their input. Earlier studies using the covariance method did not address the nature of such putative decoders.

In the case of the electrosensory system we propose a tentative decoding scheme. P-units terminate in the ELL on a number of target neurons including deep and superficial pyramidal cells (PC cells, both E and I types). The deep PC cells respond in a tonic manner to the input signal over a wide range of frequencies (they are receptor-like, Bastian et al. 2002; Bastian and Courtright 1991; Chacron 2006; Chacron et al. 2005a; b). In contrast, superficial PC cells respond in a phasic manner to the stimulus onset (Bastian and Courtright 1991) presumably because of inhibitory inputs lacking in deep PC cells (Bastian et al. 2002; Maler and Mugnaini 1994). We propose that superficial PC cells respond to the derivative of the stimulus while deep PCs respond to both the time weighted amplitude and its change. Further, we propose that midbrain neurons downstream of ELL (torus semicircularis, TS) that receive input from both deep and

superficial PC cells (Bastian et al. 2004) might subtract the superficial PC cell response from that of the deep PC cell; if the response of the deep PC cell represents E1+E2 and the superficial PC cell E2 alone, then this operation would recover E1. Although this proposal is speculative, future recording in TS should be able to confirm or refute it.

There are two constraints on this scenario. Firstly, for very low frequency input (<2Hz), both the STA and E1 become "time-smeared" due to the multiple P unit spikes per time scale of the signal (data not shown) thus invalidating the covariance method; in this case the gain is reduced because of adaptation, and the long detection times used (200 ms) encourage a rate coding approach. Secondly, for very high frequency stimuli due to electrocommunication signals, P-units synchronize (Benda et al. 2006) and averaging over P-units may no longer be effective; further, the low pass nature of I cells (Chacron 2006; Chacron et al. 2005b) means that separation by stimulus slope is no longer possible. Thus, for high frequency or transient electrocommunication signals, entirely different temporal coding strategies might be operative (Benda et al. 2006). Given these constraints and following the studies of prey capture by a closely related electric fish by Nelson and colleagues (1999) we therefore propose the following plausible sensory coding strategy. *Apteronotus* will scan for prey at velocities (>10 cm/sec) producing stimulus bandwidths ~20-30 Hz; stimulus intensities at the moment of detection are often weak, <1μV for prey >2 cm away (Bastian 1981a; Nelson and MacIver 1999; Chen et al. 2005; Babineau et al. 2006). For these frequencies there is minimal synchronization of P-units and we propose that detecting such weak signals requires estimating E1 over a large number of receptors (lateral segment of ELL) and a short period of time (<50 ms). As the fish approaches the prey, its velocity decreases (<1

cm/sec), the image width decreases, and the stimulus bandwidth accordingly decreases to <2 Hz. However the fish is also much closer to the prey (<1 cm); given the rapid drop off of stimulus intensity with distance, this implies much stronger signals (>10μV). At this point, the eigenvector decomposition no longer works since the signal's frequency is too low. However the fish, by separating the signals into positive and negative slope (via E and I PC cells), can use simple integration of P-unit input, i.e. the f_∞ or, equivalently, the 4 Hz f-I curve, to estimate the stimulus strength. For such strong, slow signals there can be averaging over a much longer time window (~200 ms) and there need not be extensive spatial averaging (~100 P units would be sufficient to detect 10 μV) and PC cells in the different ELL segments might then provide the spatially high resolution estimate of the prey's exact 3D location (Lewis and Maler 2001).

Conclusions

1. P-units can be simply modeled as independent linear rate coders with additive noise. The amount of this noise can be estimated from the variability of baseline P-unit discharge. P-units respond to the rate of change (slope) of signals as well as their intensity; the slope dependent changes in firing, mostly those associated with the rising versus falling slopes, are considered as noise sources in this simple model. A non-linear operation is therefore required to improve the rate coder: the response to up versus down-strokes of the signal must be separated by the decoder. This separation is an automatic consequence of the ELL circuitry since E and I cells encode the up and down-strokes respectively. For the relatively strong (>5μV) low frequency signals that occur during the late phases of prey capture (fish moving at <2 cm/sec and prey within <1 cm), this encoding model is adequate. Further, decoding in this case might simply be done by target (pyramidal) cell temporal integration (averaging) of the synaptic input from a moderate number of receptors.

2. This model is not adequate for the temporal bandwidth of signals present when the fish first detect prey (0 - >20 Hz and <1μV). Since the f-I curve is one dimensional, the response of the P-units to the strongly varying stimulus slope becomes an additional noise source and this overwhelms the increased gain of the receptors at higher frequencies. In this case the fish might perform an eigenvector decomposition so as to estimate the signal intensity independent of its slope; this method will permit the detection of such weak signals since, again, a biologically reasonable convergence of receptors onto pyramidal cells is adequate. There is no evidence for such computation although we have proposed a biologically plausible scheme.

Another biologically plausible, and not mutually exclusive, mechanism was recently proposed (Ludtke and Nelson 2006). Instead of treating the baseline P-unit spike train variability as noise, this method makes use of the statistical structure of the spike train and uses the conditional probabilities of spike discharge for very sensitive encoding of stimulus intensity. The authors suggest short-term plasticity of P-unit synapses onto pyramidal cells as a biologically plausible mechanism for estimating conditional probabilities. Again there is no evidence that such a computation is performed by the electrosensory system. More detailed physiological analyses of ELL and TS responses to prey signals will be required to test these hypotheses and potentially validate these sophisticated statistical methods as realistic approaches to weak signal detection by biological neural networks.

3. Electrocommunication signals can be high frequency (>30 Hz) or transient signals. Although rate coding by P-units might still contribute to encoding such signals (Benda et al. 2005), it is likely that temporal encoding by spike synchronization plays a far more important role in this case (Benda et al. 2006).

4. P values have a lognormal distribution with the majority of units with probabilities between 0.16-0.3. The coding properties of P-units vary as a function of their P value. (a) Higher P value units have lower variance than those with low P values for counting windows relevant for electrolocation (<250 ms); this is especially prominent for short counting windows (<50 ms). (b) Higher P values units have higher gain than those with lower P values (absolute spike counts only). (c) The higher P value units have a stronger E1 contribution (nearly 100%) from E1 and thus code well for the time weighted intensity; lower value P-units are better at coding for rapid changes in input

(E2). The higher gain and lower variability of the high P value units would make them very effective in detecting weak prey signals. Target neurons in ELL might therefore improve their ability to detect prey if they could selectively sample P-units with higher P values, either by selective anatomical connections or by dynamic synapses; there is no evidence that this form of optimization occurs.

P-units terminate on numerous diverse pyramidal cell types in the ELL. Further, these fish are often found in foraging groups and may therefore have to simultaneously detect a wide range of environmental and communication signal frequencies. It is therefore conceivable that multiple encoding strategies are utilised by P-units (e.g. rate, inter-spike interval and population temporal coding) and that different pyramidal cell classes differentially decode restricted codes contained within the population response: e.g. some pyramidal cells might simply integrate their P-unit input over a long time window and thus act as decoders of a rate code while others might integrate over only a single EOD cycle and thus function as synchrony detectors. The electrosensory system may therefore be an ideal preparation for investigating the difficult problem of decoding population activity for a wide range of stimuli.

Chapter 3: Discussion

The problem of neural coding by spike trains of sensory information has, since the seminal work summarized by Perkel and Bullock (1968), been central to the study of sensory systems. The electric fish has proven to be a useful model system for rigorous investigations into this problem. The research reported in this thesis suggests that the translation of environmental stimuli into an efficient neural code by the electroreceptors of the weakly electric fish, *Apteronotus leptorhynchus*, is more complex than originally thought. During foraging and hunting, these fish encounter objects with a different electrical resistivity than the ambient water: non-conductive rocks decrease the EOD amplitude while conductive prey such as Daphnia increases the EOD amplitude. These modulations of the EOD amplitude are detected by the cutaneous electroreceptors (P-units) and translated into modulations of their baseline discharge, thus forming a putative spiking rate code.

A rate code correlates firing frequency (f) with stimulus intensity (I) and this f-I relationship has been well characterized by using various forms of stimulation including sinusoidal amplitude modulations (SAMs), conductive spheres, modeling, and random amplitude modulations (RAMs) (Bastian 1981a; Wessel et al. 1996; Xu et al. 1996; Nelson et al. 1997; Ratnam and Nelson 2000; Kreiman et al. 2000; Chacron et al. 2001; Benda and Herz 2003; Benda et al. 2005; Chacron et al. 2005a; Ludtke and Nelson 2006). It appears such a rate code might be an adequate representation for the low frequency SAMs ($\leq$4 Hz) that occur during the last stages of prey detection (Nelson and MacIver 1999). This is because very long counting windows can be used and the spike count variance is minimal for such windows (Figure 1C; Ratnam and Nelson 2000) due to the

negative serial correlations of the P-unit spike train (Chacron et al. 2001). Both Bastian (1981a) and Nelson et al (1997) measured this type of neural response by stimulating with SAMs at various contrasts and frequencies. However, the intensities used were stronger than naturally experienced and had to extrapolate downwards to calculate the firing rate change for the behaviourally-relevant ~0.2uV stimulation (Knudsen et al. 1974; Rasnow 1996).

Single frequency SAMs may not be representative of the type of natural stimulus patterns these weakly electric fish encounter while exploring their natural environment. By using a random amplitude modulated (RAM) stimulus, it is possible to measure the response to behaviourally-relevant intensities with a more natural frequency content (de Ruyter van Steveninck et al. 1997). When electroreceptors are stimulated with RAMs containing the low-frequencies encountered during the final prey-capture approach, it is possible to count the number of spikes within a pre-determined time-window and correlate it to the average intensity within the same window. This time-window must be less than half the minimal period in the RAM (sampling must be at least at double the maximum stimulus frequency) due to the Nyquist frequency limit. I found that the resulting f-I relationship is linear, with a range bounded by spiking frequencies at 0 Hz and approximately double the baseline frequency of the P-unit (Figure 3A). The firing rate of P-units also depends on whether the intensity is increasing or decreasing within said time window. This dependence manifests itself as an f-I curve shift respective of the stimulus slope: the P-unit gives a stronger spiking response on the positive versus negative sloped stimulus regions, and as such the f-I curve shifts leftward (Figure 5). The variability of the spike count decreases when it was calculated separately for the stimulus

regions with positive and negative slopes as compared to when it was calculated for the entire stimulus (Figure 6). Furthermore, this method of computing the spike count also removed the bias present when counts were done irrespective of slope. This suggests that, if there was a way for the electrosensory system to perform this stimulus slope separation, the ability to confidently detect small AMs would increase.

All electroreceptor afferents converge on the primary electrosensory processing centre of the weakly electric fish's brain called the electrosensory lateral line lobe (ELL) (recent review: Maler 2007). The ELL has four adjacent segments and the three most lateral segments are innervated by P-units (Heiligenberg and Dye, 1982; Carr and Maler, 1986). These sensory neurons synapse onto two types of pyramidal cells: basilar pyramidal cells and non-basilar pyramidal cells. Basilar pyramidal cells are excited by P-unit input and are therefore called E-type; non-basilar pyramidal cells are inhibited via granule cells by the same input and are correspondingly called I-type (Bastian 1986; Metzner et al. 1998). Increasing stimulus amplitude (positive slope) will increase P-unit firing and therefore excite an E-type pyramidal. Decreasing stimulus amplitude (negative slope) will reduce P-unit firing and excite the I-type pyramidal cells (Bastian and Heiligenberg 1980; Saunders and Bastian 1984). The slope-dependent f-I relationship is equivalent to this effect since it calculates the spike rate response to either increasing (affecting E-type pyramidal cells) or decreasing (affecting I-type pyramidal cells) components of the stimulus. During the final stages of prey-capture when the prey is near the fish's skin and the EOD amplitude modulations are relatively large, this simple - yet automatic – separation of the stimulus by the sign of its slope by the E-type and I-type pyramidal cells - should be sufficient for short range navigation and prey detection. For

high frequency input that occurs during electrocommunication, a very different non-rate coding strategy might operate (Benda et al. 2006) that uses synchronization of P-unit afferents. However, investigation of this form of temporal coding was not part of my thesis research.

During the early stages of prey detection, very weak AMs with frequencies <25Hz can be generated. These frequencies do not cause substantial synchronization (Benda et al. 2006) which eliminates population correlation coding as an element of prey-capture; but to detect such frequencies using a simple counting-window coding strategy requires very short time windows and this analysis method produces very noisy results. Therefore, linear analysis techniques such as optimal stimulus reconstruction filters, coding fractions, and coherence have been used. Optimal stimulus reconstruction filters, or the spike triggered average (STA) vector, extracts an amplitude modulation (AM) in which a spike occurs when the intensity increases from a slightly negative to strongly positive modulation over a defined period of time (Figure 7A; Wessel et al. 1996). In reconstructing the stimulus, the STA vector only estimated 65-70% of the total stimulus (Wessel et al. 1996; Metzner et al. 1998; Kreiman et al. 2000). Calculation of the optimal STA was used to compute the percentage of the signal variance captured by the P-unit discharge (coding fraction) and coding fractions up to 0.80 have been reported (Wessel et al. 1996; Gabbiani and Metzner 1999; Kreiman et al. 2000). In *A. leptorhynchus* coherence has been used to demonstrate that linear encoding by P units can capture about 60-80% of the signal variability over a wide frequency range (Chacron et al. 2005); further, Chacron (2006) compared stimulus-response to response-response coherence to conclude that little additional information could be extracted by a nonlinear filter.

This thesis utilized an analytical method proposed by de Ruyter van Steveninck (1988) and used by Brenner and Bialek (2000) in the fly visual system. The covariance and eigenvector decomposition method utilized correlations of variability between spikes to detect patterns. The most prominent eigenvector (E1) from the covariance / eigenvector decomposition analysis is similar to the STA (Figure 7A) indicating that the intensity is the predominant encoded feature. This method also computed a second eigenvector (E2) whose pattern is similar to the derivative of the spike-triggered average and therefore the local stimulus slope. The linear combination of the amplitude and slope vectors (weighted by their eigenvalues) explains, on average, 92% of the total stimulus variance.

Any unaccounted variance has been associated with "noise" in the system or with the experimental methodology. System noise is the variability of the P-unit discharge rate which may be due to an imperfect receptor translation of the stimulus, a distribution variability in vesicle release (Bennett 1995), or a rate variation due to stimulus slope variability which is independent of intensity (Figure 6C). If system noise is not the cause, perhaps P-unit timing is not captured by the analysis technique. For instance, at the initial moments of detection as the fish passes a prey, the maximum cutoff stimulus frequency is significantly higher than the frequencies at the final moments of prey-capture (Nelson and MacIver 2001). Kreiman et al. (2000) determined that as the cutoff frequency of the stimulus increases so does the timing precision of the P-unit spikes in many weakly electric fish. Therefore, the unaccounted for 5-10% of the total variance from the covariance method could be due to temporal jitter in spike-timing. In the paper, the spike train was regularized to the EOD waveform to produce a binary response (presence-

absence of a spike per EOD cycle) for the covariance method and averaged within time-windows for the f-I curve analysis, removing the temporal jitter and perhaps adding noise.

The coding properties of the P-unit depend on the baseline firing rate or P-value. The P-unit's baseline activity directly influences the variance within short time-windows; the gain of the response; and the sensitivity to a particular stimulus component (time-weighted intensity versus slope). For instance, low P-value neurons are more sensitive to changes in the stimulus rather than the intensity. It is therefore not surprising there is a larger proportion of low P-value probability coding sensory neurons (see log-normal p-unit population distribution, Figure 1A, B) to ensure the 200ms response time (Nelson and MacIver 1999).

The results also suggest a plausible coding scheme different from the intensity-independent noise (i.e. constant noise) model suggested by Bastian (1981a) and Nelson et al. (1997). Such a model ensures that the probability to detect behaviourally-important signal modulations of ~0.2μV is constant despite the EOD amplitude. However, when the first eigenvector (E1) was projected onto the spike train, there was not only a linear relationship between signal similarity (or %I) and probability of spiking (or spike rate) (Figure 9B), but also a linear relationship between the spike rate variance and the relative intensity (%I) (Figure 9A). This means that at reduced EOD amplitudes, not only is the spike rate smaller, but the spike rate variance is also smaller. Since the spiking SD directly affects the detection sensitivity or the number of neurons needed to detect an intensity change (as per the calculations noted in the paper), by foraging near river beds and rocks (Nelson and MacIver 1999) these fish could either use fewer neurons to detect

behaviourally-important signals of ~0.2μV, or that these fish are in fact more sensitive to changes in intensity (less than 0.2μV) than previously calculated.

These eigenvector coding results have been seen in several other sensory systems such as visual (Brenner et al 2000), auditory (Slee et al. 2005), the cricket cercal sensory system (Dimitrov and Gedeon 2006), and vestibular (Rabbitt 1999) where the primary eigenvector correlates with the spike-triggered average and the second eigenvector is the time-derivative of the spike-triggered average. Therefore, it can be generally concluded that many primary sensory neurons use this eigenvector decomposition and can code both primary and secondary stimulus characteristics during low-intensity sensory processing. How this information is processed in upstream neurons is still unknown, but it should not be surprising then that, because of the anatomical similarities between the ELL and the auditory and vestibular systems (Carr et al. 1982, 1986), sensory neuron processing should be similar as well.

Fairhall's (Fairhall et al. 2006) research using the covariance method on retinal ganglion cells of the visual system proved that this analysis does not always work so well. Our visual system is initiated with incoming light stimulating rod and cone photoreceptors. Rods are used to see at low levels of light and cones distinguish color at daylight levels of light. These photoreceptors synapse directly onto various types of bipolar cells, which in turn synapse onto and stimulate retinal ganglion cells (Wassle 2004). There are also two classes of interneurons: horizontal cells that modulate photoreceptor-to-bipolar cell transmission; and many classes of amacrine cells that regulate bipolar-to-ganglion cells information transfer. Therefore the circuitry is already more complex than is the case of the other systems studied with this method. There are

approximately 10-15 morphologically and functionally distinct classes of retinal ganglion cells (Wassle 2004) that then transmit information to various CNS targets including (after a relay in the thalamus) the visual cortex. Basically: retinal ganglion cells are the third processing step downstream from the originating sensory photoreceptor.

Fairhall et al. recorded only a subset of the ganglion cell types (4), and only one retinal ganglion cell type had eigenvectors equivalent to the stimulus intensity and its time-derivative that corresponded with the two largest eigenvalues. The remaining three cell types had three or more large eigenvalues and the associated eigenvectors were difficult to interpret: some ganglion cells had primary eigenvectors that were time-derivatives of the STA, whereas other cells had eigenvectors completely unrelated to the STA. In other words, there are some potential limitations of the linear decomposition of the input-output relation via the covariance method as higher order cells (including those in the visual cortex) are often highly nonlinear and extracting relevant signal components may require a more sophisticated method involving information theory - this is beyond the scope of my thesis.

The general coding principle evidenced within this paper relies on the concept that a primary sensory neuron's firing rate depends on both the intensity and the change of intensity. It is the degree of dependence (the relative size of the first and second eigenvalues) that may differ between various types of receptors. Given the similarities in comparison to other model systems, along with the ease of use and other characteristics mentioned previously, the electric fish's continues to be a useful preparation for neural coding studies.

References

Abbott LF and Sejnowski TJ. eds.(1999) Neural Codes and Distributed Representations: Foundations of Neural Computation. MIT Press, Cambridge, MA. pp. vii-xiii.

Abbott LF, Varela JA, Sen K, and Nelson SB. (1997) Synaptic depression and cortical gain control. *Science* 275: 220-224.

Adrian ED. (1932) *The Mechanism of Nervous Action.* Oxford: Oxford University Press.

Albert JS and Crampton WGR. (2005) Diversity and phylogeny of Neotropical electric fishes (Gymnotiformes) In: *Electroreception* (Eds. T.E. Bullock, C.D. Hopkins, A. N. Popper, F.R. Fay). Cornell University Press, Ithaca. pp. 360-403.

Arnegard ME, Jackson BS, Hopkins CD. (2006) Time-domain signal divergence and discrimination without receptor modification in sympatric morphs of electric fishes. *J. Exp Biol.* 209: 2181-2198.

Assad C, Rasnow B, Stoddard PK. (1999) Electric organ discharges and electric images during electrolocation. *J. Exp. Biol.* 202:1185-1193.

Attneave F. (1954) Some informational aspects of visual perception. *Psychol Rev.* May; 61(3):183-93..

Babineau D, Longtin A, and Lewis JE. (2006) Modeling the electric field of weakly electric fish. *J Exp Biol.* 209: 3636-3651.

Bair W, and Koch C. (1996) Temporal precision of spike trains in extrastriate cortex of the behaving macaque monkey. *Neural Comput.* Aug 15;8(6):1185-202.

Barlow HB. (1961) Possible principles underlying the transformation of sensory messages. In *Sensory Communication*, W.A. Rosenblith, ed. (Cambridge, MA: MIT Press), pp. 217–234

Bass AH, Denizot JP, Marchaterre MA. (1986) Ultrastructural features and hormone-dependent sex differences of mormyrid electric organs. *J Comp Neurol.* Dec 22;254(4):511-28.

Bastian J. (1986a) Gain control in the electrosensory system mediated by descending inputs to the electrosensory lateral line lobe. *J Neurosci* 6: 553–562.

Bastian J. (1986b) Gain control in the electrosensory system: a role for the descending projections to the electrosensory lateral line lobe. *J Comp Physiol [A]* 158:505–515, 1986b.

Bastian J. (1999) Plasticity of feedback inputs in the apteronotid electrosensory system. *J Exp Biol* 202: 1327–1337.

Bastian J, Heiligenberg W. (1980) Phase-sensitive midbrain neurons in Eigenmannia: neural correlates of the jamming avoidance response. *Science* Aug 15;209(4458):828-31.

Bastian J, and Courtright J. (1991) Morphological correlates of pyramidal cell adaptation rate in the electrosensory lateral line lobe of weakly electric fish. *J. Comp. Physiol. A-Sensory Neural & Behavioral Physiology* 168: 393-407.

Bastian J, Chacron MJ, and Maler L. (2002) Receptive field organization determines pyramidal cell stimulus-encoding capability and spatial stimulus selectivity. *J Neurosci* 22: 4577-4590.

Bastian J, Chacron MJ, and Maler L. (2004) Plastic and nonplastic pyramidal cells perform unique roles in a network capable of adaptive redundancy reduction. *Neuron* 41: 767-779.

Bastian J, Schneiderjen S, and Nguyenkim J. (2001) Arginine vasotocin modulates a sexually dimorphic communication behavior in the weakly electric fish, *Apteronotus leptorhynchus. J. Exp. Biol.* 204: 1909-1923.

Bastian J. (1976) Frequency response characteristics of electroreceptors in weakly electric fish (Gymnotidei) with a pulse discharge, *J. Comp. Physiol. A* 112:165–180.

Bastian J. (1977) Variations in the frequency response of electroreceptors dependent on receptors location in weakly electric fish (Gymnotidei) with a pulse discharge, *J. Comp. Physiol. A*. 121:53–64.

Bastian J. (1981a) Electrolocation I. How the electroreceptors of *Apteronotus albifrons* code for moving objects and other electrical stimuli. *J Comp Physiol A* 144: 465-479.

Bastian J. (1981b) Electrolocation II. The effects of moving objects and other electrical stimuli on the activities of two categories of posterior lateral line lobe cells in *Apteronotus albifrons. J Comp Physiol A* 144: 481-494.

Benda J, and Herz AV. (2003) A universal model for spike-frequency adaptation. *Neural Comput* 15: 2523-2564.

Benda J, Longtin A, and Maler L. (2005) Spike-frequency adaptation separates transient communication signals from background oscillations. *J Neurosci* 25: 2312-2321.

Benda J, Longtin A, and Maler L. (2006) A synchronization-desynchronization code for natural communication signals. *Neuron* 52: 347-358.

Bennett MR. (1995) The origin of Gaussian distributions of synaptic potentials. *Prog Neurobiol.* 46(4):331-50.

Bennett MVL. (1970) Comparative hystology: Electric organs. *Ann. Rev.Physiol.* 32:471-475.

Bennett MVL, C Sandri, K Akert. (1998) Fine structure of the tuberous electroreceptor of the high-frequency electric fish, Sternarchus. *J. Neurocytology.* 18(2):265-283.

Bennett MVL, Obara S. (1986) Ionic mechanisms and pharmacology of electroreceptors. In: *Electroreception.* Wiley, New York.

Bennett MV. (1971) Electric organs, in: W.S. Hoar, D.J. Randall (Eds.), *Fish Physiology*, Academic Press, London, pp347-491.

Bennett MV, Sandri C, and Akert K. (1989) Fine Structure of the tuberous electroreceptor of the high-frequency electric fish, *Sternachus albifrons* (gymnotiformes). *J. Neurocytology* 18: 265-283.

Berman NJ and Maler L. (1999) Neural architecture of the electrosensory lateral line lobe: adaptations for coincidence detection, a sensory searchlight and frequency-dependent adaptive filtering. *J Exp Biol* 202: 1243–1253.

Berry MJ, Warland DK, and Meister M. (1997). The structure and precision of retinal spike trains *Proc. Natl. Acad. Sci. USA.* 94:5411–5416.

Blake RW. (1983) Swimming in the electric eels and knifefishes. *Can. J. Zool.* 61:1432–1441.

Bratton B, Bastian J. (1990) Descending Control of Electroreception. Il. Properties of Nucleus Praeeminentialis Neurons Projecting Directly to the Electrosensory Lateral Line Lobe. *J Neurosci*, 70(4): 1241-1253.

Brenner N, Bialek W, and de Ruyter van Steveninck R. (2000) Adaptive Rescaling Maximizes Information Transmission. *Neuron* 26: 695-702.

Bullock TH, Chichibu S. (1965) Further Analysis of Sensory Coding in Electroreceptors of Electric Fish. *Science.* 148(3670):664 - 665

Bullock TH. (1969) Species differences in effect of electroreceptor input on electric organ pacemakers and other aspects of behavior in electric fish. *Brain Behav Evol* 2:85–118.

Bullock TH. (1970) Sensitivity of electroreceptors. *Neurosci Res Program Bull.* 8(5):504-5

Bullock TH, Hamstra Jr RH, Scheich H. (1972) The jamming avoidance response of high frequency electric fish. *J Comp Physiol A.* 77(1):23-48

Bullock TH, Behrend K, Heiligenberg W. (1975) Comparison of the jamming avoidance responses in Gymnotoid and Gymnarchid electric fish: A case of convergent evolution of behavior and its sensory basis. *J. Comp. Physiol. A*, 103(1): 97-121.

Bullock TH. (1982) Electroreception *Ann. Rev. Neurosci.* 5:121-70.

Caputi A, Budelli R, Grant K, and Bell CC (1998). The electric image in weakly electric fish: physical images of resistive objects in *Gnathonemus petersii. J. Exp. Biol.* 201, 2115–2128.

Caputi AA, Castello ME, Aguilera P, Trujillo-Cenoz O. (2002) Electrolocation and electrocommunication in pulse gymnotids: signal carriers, pre-receptor mechanisms and the electrosensory mosaic. *J. Physiol. Paris,* 96:493–505.

Carr CE, Maler L, Heiligenberg W, Sas E. (1981) Laminar Organization of the Afferent and Efferent Systems of the Torus Semicircularis of Gymnotiform Fish: Morphological Substrates for Parallel Processing in the Electrosensory System. *J. Comp. Neurol.,* 203:649-670.

Carr CE, Maler L. (1985) A Golgi Study of the Cell Types of the Dorsal Torus Semicircularis of the Electric Fish *Eigenmannia:* Functional and Morphological Diversity in the Midbrain. *J. Comp. Neurol.*, 235:207-240.

Carr CE, Maler L. (1986) A Time-Comparison Circuit in the Electric Fish Midbrain II. Functional Morphology. *J Neurosci.*, 6(5):1372-1383.

Carr CE, Maler L, and Sas E. (1982) Peripheral organization and central projections of the electrosensory organs in gymnotiform fish. *J. Comp. Neurol.,* 211: 139-153.

Chacron MJ, Longtin A, and Maler L. (2001) Negative interspike interval correlations increase the neuronal capacity for encoding time-dependent stimuli. *J. Neurosci.,* 21: 5328-5343.

Chacron MJ, Maler L, and Bastian J. (2005a) Electroreceptor neuron dynamics shape information transmission. *Nat Neurosci* 8: 673-678.

Chacron MJ, Maler L, and Bastian J. (2005b) Feedback and feedforward control of frequency tuning to naturalistic stimuli. *J. Neurosci.,* 25: 5521-5532.

Chacron MJ. (2006) Nonlinear information processing in a model sensory system. *J. Neurophysiol.,* 95:2933-2946.

Chen L, House JL, Krahe R, and Nelson ME. (2005) Modeling signal and background components of electrosensory scenes. *J. Comp. Physiol. A,* 191: 331-345.

Coombs S, New JG, Nelson M. (2002) Information-processing demands in electrosensory and mechanosensory lateral line systems. *J. Physiol. Paris*, 96(5-6):341-54.

Dayan P, and Abbott L. (2001) Theoretical Neuroscience. MIT Press, Cambridge, MA. p.576.

de Boer E., and Kuyper P. (1968). Triggered correlation. *IEEE Trans. Biomed. Eng. 15*, 169–179.

de Ruyter van Steveninck RR, Lewen GD, Strong SP, Koberle R, and Bialek W. (1997). Reproducibility and variability in neural spike trains. *Science,* 275:1805–1808.

de Ruyter van Steveninck RR, and Bialek W. (1988) Real-time performance of a movement sensitive neuron in the blowfly visual system: coding and information transfer in short spike sequences. *Proc. Royal Soc. London B. Biol. Sci.,* 234: 379-414.

DeAngelis GC, Ohzawa I, Freeman RD. (1995) Receptive-field dynamics in the central visual pathways. *Trends Neurosci.,* 18:451–58.

DeCharms RC and Zador A. (2000) Neural representation and the cortical code. *Annu. Rev. Neurosci.,* 23:613-647.

deCharms RC. (1998) Information coding in the cortex by independent or coordinated populations. *Proc. Natl. Acad. Sci. USA,* 95: 15166–68.

DiCarlo JJ, Johnson KO. (1999) Velocity invariance of receptive field structure in somatosensory cortical area 3b of the alert monkey. *J. Neurosci.,* 19:401–19.

Dimitrov AG, Gedeon T. (2006) Effects of stimulus transformations on estimates of sensory neuron selectivity. J. Comput. Neurosci., 20:265–283

Engler G, Fogarty CM, Banks JR, Zupanc GKH. (2000) Spontaneous modulations of the electric organ discharge in the weakly electric fish, *Apteronotus leptorhynchus*: a biophysical and behavioral analysis. *J. Comp. Physiol A.* 186 (7):645-660.

Fairhall AL, Burlingame CA, Narasimhan R, Harris RA, Puchalla JL, and Berry MJ 2nd. (2006) Selectivity for multiple stimulus features in retinal ganglion cells. *J. Neurophysiol.*, 96: 2724-2738.

Frey AH, Eichert ES. (1972) The Nature Of Electrosensing In The Fish. *Biophysical Journal*, 12:1326-1358.

Gabbiani F, Koch C. (1996) Coding of Time-Varying Signals in Spike Trains of Integrate-and-Fire Neurons with Random Threshold. *Neural Computation,* 8(1):44-66.

Gabbiani F, Metzner W. (1999) Encoding and Processing Of Sensory Information In Neuronal Spike Trains. *J. Exp. Biol.,* 202:1267–1279.

Gabbiani F. (1996) Coding of time-varying signals in spike trains of linear and half-wave rectifying neurons. *Network: Computation in Neural Systems,* 7: 61-85.

Gaudry KS, Reinagel P. (2007) Benefits of Contrast Normalization Demonstrated in Neurons and Model Cells. *J. Neurosci.,* 27(30):8071– 8079.

Goense JB, and Ratnam R. (2003) Continuous detection of weak sensory signals in afferent spike trains: the role of anti-correlated interspike intervals in detection performance. *J. Comp. Physiol. A,* 189: 741-759.

Heiligenberg W, Bastian J. (1984) The Electric Sense of Weakly Electric Fish. *Annual Review of Physiology*, 46:561-583.

Heiligenberg W. (1977) Principles of Electrolocation and Jamming Avoidance in Electric Fish, a Neuroethological approach. Braitenberg V (ed) *Studies of brain function, vol 1.* Springer, Berlin, Heidelberg, New York.

Heiligenberg W, Dye J. (1982) Labelling of electroreceptive afferents in a gymnotoid fish by intracellular injection of HRP: The mystery of multiple maps. *J. Comp. Physiol. A*, 148(3):287-296.

Heiligenberg W, and Rose G. (1985) Phase and Amplitude Computations in the Midbrain of an Electric Fish: Intracellular Studies of Neurons Participating in the Jamming Avoidance Response of Eigenmannia. *J. Neurosci.,* 5(2):515-531.

Heiligenberg W, and Partridge BL. (1981) How electroreceptors encode JAR eliciting stimulus regimes: reading trajectories in a phase amplitude plane. *J. Comp. Physiol.,* 142: 295-308.

Heiligenberg W. (1980) The Jamming Avoidance Response in the weakly electric fish *Eigenmannia. Naturwissenschaften,* 67:499-507.

Heiligenberg W. (1991) Neural nets in electric fish. Published: MIT Press, Cambridge, MA.

Hoekstra D, Janssen J. (1986) Lateral Line Receptivity in the Mottled Sculpin (Cottus bairdi). *Copeia,* 1:91-96.

Hopkins CD. (1976) Stimulus filtering and electroreception: Tuberous electroreceptors in three species of Gymnotid fish. *J. Comp. Physiol.,* 111 : 171-207

Hoshimiya N, Shogen K, Matsuo T, Chichibu S. (1980) The *Apteronotus* EOD field: Waveform and EOD field simulation. *J. Comp. Physiol.,* 135 : 283-290

Isokawa M. (1997) Membrane time constant as a tool to assess cell degeneration. *Brain Res. Protoc.,* 1:114-116.

Jones JP, Palmer LA. (1987) The two-dimensional spatial structure of simple receptive fields in cat striate cortex. *J. Neurophysiol.,* 58:1187–211.

Knudsen E. (1974) Behavioral thresholds to electric signals in high frequency electric fish. *J. Comp. Physiol.,* 91: 333-353.

Kramer, B. (1990). Electrocommunication in Teleost Fishes: Behavior and Experiments. Berlin: Springer-Verlag.

Kramer B, Tautz J, Markl H. (1981) The EOD sound response in weakly electric fish. *J. Comp. Physiol. A*, 143(4):435-441

Kreiman G, Krahe R, Metzner W, Koch C, and Gabbiani F. (2000) Robustness and variability of neuronal coding by amplitude-sensitive afferents in the weakly electric fish *Eigenmannia. J. Neurophysiol.,* 84: 189-204,.

Lewis J, Maler L. (2003) Dynamics of Electrosensory Feedback: Short-term plasticity and Inhibition in a Parallel Fiber Pathway. *J. Neurosci.,* 88:1695-1706.

Lewis JE, Maler L. (2001) Neuronal population codes and the perception of object distance in weakly electric fish. *J. Neurosci.,* 21: 2842–2850.

Lissmann HW, Machin KE. (1958) The Mechanism of Object Location in *Gymnarchus Niloticus* and Similar Fish. *J. Exp. Biol.,* 35:451-486.

Ludtke N, and Nelson ME. (2006) Short-term synaptic plasticity can enhance weak signal detectability in nonrenewal spike trains. *Neural Comput.,* 18: 2879-2916.

MacIver MA, Sharabash NM, and Nelson ME. (2001) Prey capture behavior in gymnotid electric fish: motion analysis and effects of water conductivity. *J. Exp. Biol.,* 204: 543-557.

Mainen ZF and Sejnowski TJ. (1996) Influence of dendritic structure on firing pattern in model neocortical neurons. *Nature,* 382: 363–366.

Maler L, and Mugnaini E. (1994) Correlating gamma-aminobutyric acidergic circuits and sensory function in the electrosensory lateral line lobe of a gymnotiform fish. *J. Comp. Neurol.,* 345: 224-252.

Maler L, Sas EK, and Rogers J. (1981) The cytology of the posterior lateral line lobe of high frequency weakly electric fish (*Gymnotoidei)*: Dendritic differentiation and synaptic specificity in a simple cortex. *J. Comp. Neurol.,* 195: 87-139.

Maler L. (1979) The posterior lateral line lobe of certain gymnotoid fish: quantitative light microscopy. *J. Comp. Neurol.,* 183: 323–363.

Maler, L. (2007) Neural Strategies for optimal processing of sensory signals, *Prog. Brain Res.*, 165:135-154.

Mechler F, Victor JD, Purpura KP, Shapley R. (1998) Robust temporal coding of contrast by V1 neurons for transient but not for steady-state stimuli. *J. Neurosci.,* Aug 15;18(16):6583-98.

Metzner W, Koch C, Wessel R, and Gabbiani F. (1998) Feature extraction by burst-like spike patterns in multiple sensory maps. *J. Neurosci.,* 18: 2283–2300.

Metzner W. (1999) Neural circuitry for communication and jamming avoidance in gymnotiform electric fish. *J. Exp. Biol.* 202(10):1365-75.

Moortgat KT, Keller CH, Bullock TH, and Sejnowski TJ. (1998) Submicrosecond pacemaker precision is behaviorally modulated: the gymnotiform electromotor pathway. *Proc. Natl. Acad. Sci. USA,* 95: 4684-4689.

Nelson ME, and MacIver MA. (1999) Prey capture in the weakly electric fish *Apteronotus leptorhynchus*: sensory acquisition strategies and electrosensory consequences. *J. Exp. Biol.,* 202: 1195-1203.

Nelson ME, Xu Z, and Payne JR. (1997) Characterization and modeling of P-type electrosensory afferent responses to amplitude modulations in a wave-type electric fish. *J. Comp. Physiol. A,* 181: 532–544.

Nelson ME. (2005) Target detection, image analysis, and modeling. In: *Electroreception*, edited by Bullock TH, and Hopkins CD. New York: Springer, p. 290-317.

Oswald AM, Chacron MJ, Brent Doiron, BastianJ, and Maler L. (2004) Parallel Processing of Sensory Input by Bursts and Isolated Spikes. *J. Neurosci.*, 24(18):4351–4362.

Pappas GD, Waxman SG. (1972) Synaptic fine structure—morphological correlates of chemical and electrotonic transmission. In *Structure and Function of Synapses*, ed. GD Pappas, DP Purpura, pp. 1–43. New York: Raven.

Parker AJ, Newsome WT. (1998) Sense and the single neuron: probing the physiology of perception. *Annu. Rev. Neurosci.,* 21:227-77.

Perkel D, and Bullock TH. (1968) Neural Coding. In: *Neuroscience Research Program.* Cambridge, Mass.: MIT Press.

Popper AN and Platt C. (1993) Inner ear and lateral line, in *The Physiology of Fishes*, 1st ed. (CRC Press).

Rabbitt RD. (1999) Directional coding of three-dimensional movements by the vestibular semicircular canals. *Biol. Cybern.*, 80, 417-431.

Rasnow B. (1996) The effects of simple objects on the electric field of *Apteronotus. J. Comp. Physiol. A.*, 178:397-411.

Ratnam R, and Nelson ME. (2000) Non-renewal statistics of electrosensory afferent spike trains: implications for the detection of weak sensory signals. *J. Neurosci.,* 20:6672-6683.

Reid RC, Alonso JM. (1995) Specificity of monosynaptic connections from thalamus to visual cortex. *Nature,* 378:281–84.

Reid RC, Soodak RE, Shapley RM. (1991) Directional selectivity and spatiotemporal structure of receptive fields of simple cells in cat striate cortex. *J. Neurophysiol.,* 66:505–29.

Rieke F, Warland D, de Ruyter van Steveninck RR, Bialek W. (1997) *Spikes: Exploring the Neural Code.* Cambridge, MA: MIT Press.

Ringach DL, Hawken MJ, Shapley R. (1997) Dynamics of orientation tuning in macaque primary visual cortex. *Nature,* 387:281-84.

Ruderman DL, Bialek W. (1994) Statistics of natural images: Scaling in the woods. *Phys. Rev. Lett., 73:814 – 817.*

Sachs MB. (1984) Neural Coding of Complex Sounds: Speech. *Ann. Rev. Physiol.*, 46: 261-273.

Sas E and Maler L. (1983) The nucleus Praeeminentialis: a Golgi study of a feedback center in the electrosensory system of a gymnotid fish. *J. Comp. Neurol.,* 221: 127–144.

Sas E and Maler L. (1987) The organization of afferent input to the caudal lobe of the cerebellum of the gymnotid fish *Apteronotus leptorhynchus. Anat. Embryol.,* 177: 55–79.

Saunders J and Bastian J. (1984) The physiology and morphology of two types of electrosensory neurons in the weakly electric fish *Apteronotus leptorhynchus. J. Comp. Physiol. A,* 154: 199–209.

Scheich J, Bullock TH (1974) The detection of fields from electric organs. In: *Handbook of sensory physiology*. Springer, New York.

Scheich H, Ebbesson SOE. (1983) Inputs to the torus semicircularis in the electric fish *Eigenmannia virescens. Cell and Tissue Research*, 215(3):531-536.

Scheich H, Bullock TH, Hamstra Jr RH. (1973) Coding Properties of Two Classes of Afferent Nerve Fibers: High-Frequency Electroreceptors in the Electric Fish, *Eigenmannia. J. Neurophysiol.*, 36:39-60.

Scheich H. (1977) Neural basis of communication in the high frequency electric fish, *Eigenmannia virescens* (jamming avoidance response). *J. Comp. Physiol.,* 113:181-255.

Shumway CA and Maler L. (1989) GABAergic inhibition shapes temporal and spatial response properties of pyramidal cells in the electrosensory lateral line lobe of gymnotiform fish. *J. Comp. Physiol. A,* 164: 391–407.

Singer W. (1999) Neuronal synchrony: a versatile code for the definition of relations? *Neuron,* 24:49–65.

Slee SJ, Higgs MH, Fairhall AL, and Spain WJ. (2005) Two-dimensional time coding in the auditory brainstem. *J. Neurosci.,* 25: 9978-9988.

Stoddard PK. (2002) The evolutionary origins of electric signal complexity. *J Physiol. Paris,* 96:485–491.

Theunissen F, Miller JP. (1995) Temporal Encoding in Nervous Systems: A Rigorous Definition. *J. Comp. Neurosci.*, 2:149-162.

Viancour TA. (1979) Electroreceptors of a weakly electric fish. *J. Comp. Physiol. A*, 133(4):327-338.

von der Emde G. (1999) Active electrolocation of objects in weakly electric fish. *J. Exp. Biol.*, 202(10):1205-1215.

von der Emde G, Bleckmann H. (1998) Finding food: senses involved in foraging for insect larvae in the electric fish Gnathonemus petersii. *J. Exp. Biol.*, 201(7):969-980l.

Warzecha AK, Kretzberg J, Egelhaaf M. (1998) Temporal precision of the encoding of motion information by visual interneurons. *Curr. Biol.*, 8(7):359-68.

Wassle H. (2004) Parallel processing in the retina. *Nat. Rev. Neurosci.*, 5: 747-757.

Wessel R, Koch C, and Gabbiani F. (1996) Coding of time-varying electric field amplitude modulations in a wave-type electric fish. *J. Neurophysiol.,* 75: 2280–2293.

Wotton J, Ferragamo MJ, Sanderson MI. (2004) The Emergence of Temporal Hyperacuity from Widely Tuned Cell Populations. *Network: Computation in Neural Systems,* 15:159-177.

Xu Z, Payne JR, and Nelson ME. (1994) System Identification and Modeling of Primary Electrosensory Afferent Response Dynamics. In: *Computation in Neurons and Neural Systems*, edited by Eeckman Kluwer Academic Press, p. 197-202.

Xu Z, Payne JR, and Nelson ME. (1996) Logarithmic time course of sensory adaptation in electrosensory afferent nerve fibers in a weakly electric fish. *J. Neurophysiol.,* 76:2020-2032.

Zakon HH. (1984) Fish Neurobiology (Ed.) R.G. Northcutt and R. Davis for *Copeia*, no2. 559-560.

Zakon HH. (1986) The electroreceptive periphery. In: *Electroreception*, edited by T. H. Bullock and W. Heiligenberg, New York: John Wiley and Sons, p. 103-156.

Zakon HH, Oestreich J, Tallarovic S, and Triefenbach F. (2002) EOD modulations of brown ghost electric fish: JARs, chirps, rises, and dips. *J Physiol Paris,* 96: 451-458.

Zohary E, Shadlen MN, Newsome WT. (1994). Correlated neuronal discharge rate and its implications for psychophysical performance. *Nature,* 370:140 – 143.